HEDL-SA-2321 FP
CONF-810606--65

MASTER

FUELS AND MATERIALS FOR LMFBR'S

C. M. Cox
R. J. Jackson
J. L. Straalsund

American Nuclear Society Annual Meeting

June 7-12, 1981 - Miami Beach, Florida

HANFORD ENGINEERING DEVELOPMENT LABORATORY
Operated by Westinghouse Hanford Company, a subsidiary of Westinghouse Electric Corporation, under the Department of Energy Contract No. DE-AC14-76FF02170
P.O. Box 1970, Richland, Washington 99352

FUELS AND MATERIALS FOR LMFBR's

Introduction

This paper reviews development of fuels and materials for the Liquid Metal Fast Breeder Reactor. Included are the status of fuels and materials technology for the LMFBR core components, how we got there, and a brief look at where we're headed. First is a bit of orientation. The first figure (Figure 1) shows schematically a typical LMFBR driver fuel assembly. This is the fuel assembly for the Fast Flux Test Facility, or FFTF, in operation in Richland, Washington. The outer part of the 12 foot long assembly is called a flow channel or duct. Inside are 217 fuel pins each containing mixed uranium-plutonium oxide fuel pellets. The fuel pins are spaced apart from each other in a hexagonal array by spiral wire wraps, which form flow channels among the pins. The basic structural material in this fuel assembly is cold worked AISI type 316 stainless steel. Figure 2 shows the comparable schematic for a control rod or absorber assembly. The FFTF absorber assembly contains 61 control rods containing boron carbide pellets. Because FFTF is a test reactor it does not contain blanket assemblies; however, the Clinch River Breeder Reactor blanket assemblies look very similar to the FFTF fuel assembly except that they each contain 61 UO_2 rods.

Sizes of various LMFBR fuel assemblies are compared in Figure 3. The Clinch River Breeder Reactor fuel assembly is nearly identical to that of FFTF except for an increased length to accommodate UO_2 axial blankets within the fuel pins. The DP-1 design is for a large breeder reactor and uses larger ducts and more fuel pins per assembly. By comparison, the fuel assemblies for EBR-II, where we've conducted most of our irradiation experiments are much smaller, as is the EBR-II core.

Development Program

The fuels and materials development program utilizes an historically successful iterative procedure of making performance predictions for various

materials and potential core component designs, designing laboratory and irradiation experiments to measure important properties and to determine the effects of key design variables on performance, fabricating these experiments to the extent feasible with commercially viable processes with well characterized materials, conducting experiments under controlled conditions, performing postirradiation examinations to determine the actual performance of the components and to explain any anomalies or failures, improving the performance and design codes, and repeating the process with improved materials and designs until convergence has been made on a design which will meet its objectives. This is followed with a systemmatic, statistically significant matrix of proof tests addressing both steady state irradiation performance and the transient or off-normal performance of the core components. Such a program typically requires a 15 year period. The scope of the irradiations program in EBR-II has been quite wide, as indicated in Figure 4.

Included in the fuels program have been some 3000 (U, Pu)O_2 fuel pins, approximately 450 (U, Pu)C fuel pins, 100 (U, Pu)N fuel pins, 30 (Pu, Th)O_2 and 5 (Pu, Th)C fuel pins. The blanket test program has included about 24 UO_2 pins and 12 ThO_2 pins. Emphasis continues on oxide fuel and blanket pins, with longer range activities addressing carbides. Exposures in fuel testing have been quite high, with oxide fuel pins reaching burnups up to 200,000 MWd/T, and carbide, 120,000 MWd/T. In fact, 1384 fuel pins have exceeded in EBR-II testing the 80,000 MWd/T peak design burnup of FFTF.

Control materials tested include B_4C, EuB_6, Eu_2O_3, and Ta. The B_4C material has been an outstanding performer; we've tested approximately 320 B_4C pins in EBR-II, to exposures up to 180×10^{20} captures/cm^3. Approximately 75 B_4C pins have exceeded the 45×10^{22} captures/cm^3 design burnup of the initial FFTF control assemblies.

The structural materials program has investigated myriad materials, emphasizing austenitic stainless steels but with substantial efforts on martensitic, ferritic, and precipitation strengthened alloys.

Because of the small size and low neutron flux levels in EBR-II compared to the FFTF and other large reactors, we've had to make several compromises. Figure 5 shows a typical fuel test assembly in EBR-II in which 61 FFTF-type fuel pins are tested, but the length has been shortened from the standard eight feet to approximately five feet. The fuel column length has been shortened from the reference 36 inches to EBR-II's core height of 13-1/2 inches, and since EBR-II has a peak fast neutron flux of 2×10^{15} n/cm^2-sec, compared to FFTF's 5×10^{15}, the uranium is typically enriched to provide the required power output in the fuel pins. The various tests in EBR-II have addressed a wide range of operating conditions in general exceeding the requirements of the core components but with the limitations associated with using a small test facility.

Investigations of transient performance of fuel pins have also addressed a wide spectrum, as shown in Figure 6. Again, emphasis has been on $(U,Pu)O_2$ fuel pins. Early transient tests used capsules of NaK containing fuel rods which had been irradiated in EBR-II and then subsequently pulsed in TREAT to simulate the fuel pin temperature history of rapid, overpower transients. More complicated but more prototypic TREAT tests in self contained loops of flowing sodium are now used to study fuel pin performance under the more typical conditions of slow overpower transients and loss of flow transients. A typical TREAT test loop is shown in Figure 7. TREAT test data are augmented by fuel cladding transient tests performed in the hot cells. For these tests irradiated fuel pins are cut into segments. After removal of the fuel the cladding is subjected to pressure and/or temperature ramps to simulate design transients, and the strain response or strength of the cladding is determined. The fuel cladding transient test rig is shown in Figure 8. The final complement of transient test data for developing and validating performance and design codes comes from measurements of the creep and hot pressing properties of $(U, Pu)O_2$ fuel pellets at high strain rates, to approximately 5×10^{-2} sec^{-1}, at temperatures from 2100°C to 2700°C (Figure 9).

We are now in an exciting transition in the testing program as we are starting experiments in FFTF with full size components under more prototypic conditions which are more completely and accurately measured and controlled. At the same time the mission of experiments in EBR-II is changing to emphasize slow overpower transients and continuing irradiation of fuel pins after a cladding breach has occurred. The scale up of the tests is indicated in Figure 10, which compares both size and environment for EBR-II and FFTF. FFTF not only has prototypic size conditions with flow and temperature instrumentation for each core position; it also has capability of conducting up to 8 highly instrumented tests in which the operating environment is carefully monitored and in some cases carefully controlled. Figure 11 shows schematically how an instrumented test assembly which is 40 feet in length is installed in FFTF and the instrumentation leads are fed through the reactor head. We presently have three instrumented assemblies operating in FFTF. Two are fuel test assemblies (Figure 12), and one is an absorber test assembly. The first instrumented materials test assembly has been fabricated and will be installed in FFTF early in 1982.

Ducts

The performance of LMFBR core components is strongly influenced by the behavior of the channels or ducts used in the fuel, control, and blanket assemblies. In addition to providing a flow channel which can be orificed to control temperatures, the ducts provide the basic structural components of the core. Figure 13 shows a schematic diagram of the arrangement of ducts for a radial row in the FFTF. Fuel assemblies are located through Row 6. Rows 7 and 8 are formed by reflector assemblies, and the entire group of assemblies in the core is constrained by yokes which are attached to the core vessel.

There are appreciable variations in temperature and flux both axially and radially in the core as indicated on this figure. Under the influence of fast neutron irradiation, the stainless steel duct material swells due to

the formation of voids. Figure 14 shows the effect of neutron fluence on the growth of the voids, and Figure 15 shows how the swelling from the voids is very dependent on irradiation temperature. The net effect of fluence and temperature on swelling is to cause both axial growth and bowing of the ducts, shown schematically in Figure 16. The allowable irradiation exposure of many LMFBR core components is limited by the effects of the duct distortions. There is a limit to the allowable length increase which can be accommodated with the fuel handling system. In addition, the combined effects of swelling and creep from the 30 to 60 psi internal pressure in the core region result in a bulging or dilation of the ducts. This, in combination with the bowing of the ducts because of the radial flux and temperature gradients, will eventually cause the ducts to come in contact and increase the force required to withdraw or insert assemblies during refueling.

Loads are transmitted across the core through the load pads on the ducts and eventually must be accommodated within the core restraint system. Fortunately there is a very effective stress relieving mechanism which is also caused by irradiation and which limits stresses in general to relatively low values. This is the effect of irradiation on creep as shown in Figure 17. At the moderately low temperatures and pressures at which the ducts perform there is significant in-reactor creep.

A 3-dimensional finite element model has been used to simulate the distortions and interactions of the ducts in FFTF. Predicted results after three cycles of irradiation are shown in Figure 18. Note that in the upper part of this figure, which describes the predicted distortions of the ducts at shutdown, there will be appreciable bow of the ducts and expansion in the core region. As shown in the lower part of the figure, installation of new straight assemblies requires a certain degree of core compliance. These conditions in FFTF arise after a fast neutron fluence of 1.2×10^{23} n/cm^2 compared with design fluences of 2.4×10^{23} for large LMFBR's. It is clear that a lower swelling duct material is required to achieve the higher exposures anticipated for the large LMFBR's.

Development of such low swelling alloys has been given very high priority for the past 10 years, and half a dozen low swelling steels are now available. Data for one of the promising alloys for duct application, HT9, are compared with the reference cold worked 316 stainless steel in Figures 19 and 20. Duct performance predictions (Figure 21) appear favorable for this martensitic alloy.

Fuel Pins

Lets turn now to the fuel pins, represented typically in Figure 22 by an FFTF driver fuel pin. The major difference between this particular one and the large breeder reactor pins is the addition of a foot or so of UO_2 blanket pellets above and below the stack of mixed oxide fuel pellets. Each fuel pin delivers some thirty to forty kilowatts of heat to the sodium coolant. Operating conditions as structural components are quite severe. The fuel pins operate with the cladding in a dull cherry red condition, with peak temperatures on the order of 1100°F. The fuel itself operates with peak fuel temperatures on the order of 4000°F.

Each rod contains a void space which is termed a "gas plenum". The plenum accumulates much of the inert xenon and krypton fission gases, which account for some 13% of the fission products, and hence the fuel pins become small pressure vessels. At the same time, additional quantities of gaseous and solid fission products are retained in the fuel and cause the fuel to swell. The result is that over an extended time period, there is an increase in the size of the fuel pins. Figure 23 shows the increase in diameter with neutron fluence that we have observed with fuel pins clad with type 316 stainless steel. In the case shown, some two thirds of the increase was due to void-induced swelling of the stainless steel cladding. The remainder of the increase was due to combination of creep due to the fission gas pressure, or to the loading of the swelling fuel. Under most conditions, the FFTF driver fuel pins will not experience a significant fuel swelling loading on the cladding. This is achieved by fabricating the fuel with approximately 10%

porosity, and in addition, providing a gap or space between the fuel pellets and the cladding, which together accommodate the fuel swelling internally. However, in some tests aimed at demonstrating the performance under extremely high burnup conditions or under conditions where there is higher effective fuel density, we have seen indications of mechanical interaction loads.

One significant problem which arose during the test program in EBR-II, was that a number of the 61 pin test assemblies experienced a significant vibration of the pin bundles, such that a severe wear occurred between the wire wrap spacer on fuel pins, and the cladding surface on adjacent pins. A typical example is shown in Figure 24. This was avoided in subsequent tests by reducing the as-fabricated clearance between the fuel pin bundle and the duct.

Due to the high operating temperatures and temperature gradients, it is well known that the oxide fuel undergoes an in-reactor densification or restructuring as shown in Figure 25. Fuel restructuring has a marked effect on many of the steady state and transient performance characteristics of the fuel pins. In addition to densification, fuel restructuring includes fuel cracking and healing of the cracks, which in conjunction with fuel swelling, tends to close the gap between fuel and cladding. The densification, gap closure and migration of pores up the radial temperature gradient of the fuel tend to form a central cavity or central void in the fuel pellet and together result in a lowering of the fuel operating temperature.

One concern related to densification is to avoid significant changes in fuel column length so as not to cause any perturbations to core reactivity. This has been addressed by developing fabrication techniques which minimize the amount of submicron porosity in the fuel. It is the small pores which are sensitive to radiation enhanced dissolution, resulting in fuel shrinkage.

The behavior of the fission product gases is strongly influenced by the temperature distribution of the fuel, and as a result the amount of gas which

is released to the fission gas plenum varies as a function of both burnup and linear heat rate, as shown in Figure 26. The remaining gases are retained in the fuel, and these contribute to fuel swelling during both normal and transient operating conditions. With the formation of fission products, the oxygen activity in the mixed oxide fuel pin continuously increases, such that eventually there will be a reaction between the fuel and the cladding. The reaction is significantly dependent on the stoichiometry of the fuel and on the cladding temperature and burnup. This reaction is controlled and maintained at a low level by fabricating the fuel in a hypostoichiometric condition. A typical reaction product is shown in Figure 27. Although intergranular attack in the cladding is sporadically observed, generally at lower burnup levels and higher fuel O/M values, the most common form of the reaction is a matrix reaction as shown in this figure.

Fuel pin power limits are typically set in design by a requirement to maintain a certain margin between the fuel pin linear heat rate and that local heat rate which would correspond to incipient fuel melting at the center of the fuel pellets. The latter is called the "linear heat rating to melting." This has been determined by direct in-reactor experiments where the fuel has been overpowered, and destructive examinations were used to relate local heat rate to the axial extents of fuel melting along the centerline of the fuel pins. Such data have been developed (Figures 28 and 29) as a function of fuel-to-cladding gap, and to a limited extent as a function of fuel burnup. A recent experiment, not yet examined, extended the variables to include fuel pin diameter. Kinetics of fuel temperature change with time have been determined by calibrating fuel pin thermal performance models to power-to-melt and restructuring measurements and to in-reactor measurements of fuel temperature (Figure 30).

Many of the experiments in EBR-II were purposely conducted to very high exposures or burnups to determine the failure characteristics of the fuel pins. This was called a "run-to-cladding-breach" program. Microstructures

of a typical cladding failure are shown in Figure 31. The failures are commonly associated with local cladding hot spots which may have been experimental anomolies. The cladding breaches are characterized by a very slow release of fission gases which are detected in the reactor cover gas system. When the fuel pins are later examined, the breaches are very difficult to locate and generally have to be found by internal pressurization of the fuel pins immersed in liquid. Fuel pin cladding breaches which occur at higher temperatures show cavitation creep failures and higher failure strength and ductility, fairly typical of the intrinsic cladding properties (Figure 32). Under these conditions cumulative creep strain or creep rupture analysis techniques appear appropriate for predicting fuel pin lifetime. However, at lower irradiation temperatures, the breaches exhibit a low strength, low ductility intergranular fracture mechanism which may be the result of fission product assisted crack propagation along embrittled cladding grain boundaries (Figure 33).

Several experiments have been deliberately operated for some period after failure, in a run-beyond-cladding-breach mode. The objectives of these experiments were to relate changes in the fuel pin failure geometry to the delayed neutron signals in the reactor and to determine the margin for operation under these conditions. It appears that fuel pins can be operated for extended time periods after a breach with little effect until sodium enters the pin. Subsequent operation at power results in a sodium-fuel reaction which expands the cladding fissure. Figure 34 shows a typical example of the effect of continued operation after a fuel pin failure and sodium-fuel reaction.

Altogether, this phase of the development program demonstrated a high burnup capability for the oxide fuel. It determined the power limits through a series of power-to-melt tests. It also demonstrated that fuel pin failures, when they occur, are benign. Fuel fabrication techniques have been developed to minimize chemical reactions between fuel and cladding and to provide dimensionally stable fuel.

Significant numbers of transient tests have been conducted on the fuel pins irradiated in EBR-II. These have taken three basic forms: First a series of experiments were conducted in TREAT to simulate the design basis transients for FFTF. The second series of tests was aimed at determining fuel pin failure thresholds. The third series of tests studied the mechanical properties of sections of cladding from irradiated fuel pins.

Thirty-one rapid overpower transient tests have been conducted in TREAT with mixed-oxide fuel pins at various burnup levels. These demonstrated that the FFTF fuel pin can take significantly more severe transients than those possible with the plant protective system (Figure 35). From failure threshold results or "unterminated" transient tests it has been determined that cladding breach for fast transients is usually the result of molten fuel expansion, possibly combined with fission gas induced swelling in irradiated fuel or fuel vapor pressurization in unirradiated or low burnup fuel. Failure will most likely occur in the upper half of the fuel column at a location where there is little or no central void and where the fuel has an intermediate power structure typical of incipient central void formation.

Slower ramp transients may be more damaging to pin performance than faster ramp transients. This is due to a combination of higher stresses due to higher fuel temperatures and weaker cladding properties (Figure 36). As a result, accurate assessments of fuel expansion and of fuel stress relieving phenomena such as fuel creep and hot pressing are important in evaluating and predicting performance.

The fuel-cladding-transient tests started with the objective of determining performance of fuel pins under loss-of-flow transient conditions, where fuel-cladding mechanical interactions should not be significant. These tests soon determined that the strength of irradiated cladding sections which had been adjacent to fuel was significantly less than that of cladding irradiated in the absence of fuel (Figure 37). As a result extensive experiments were conducted to determine relevant cladding properties. These data are now being extended to higher fluences.

On the whole, the transient testing activity indicates that the FFTF fuel pin will satisfy its design objectives, but there are still open issues relating to slow overpower transients and to the performance of full length irradiated fuel pins from FFTF.

Absorbers

The favored control mechanism for todays LMFBR's is use of movable B_4C rods. Control rod guide tubes in the instrument tree and the absorber assemblies installed in FFTF core are shown in Figure 38, which was taken during FFTF construction. The reference FFTF absorber assembly is a 61-sealed pin design with 316 SS 20% CW cladding. Testing is underway of a 19-vented pin design with D9 20% CW cladding and ducts. These designs are shown in Figure 39. In both designs, a major lifetime limiter is swelling of the boron carbide relative to the cladding.

The development program has concentrated on characterizing the swelling and gas release performance of the boron carbide absorber material in the fast reactor systems. Many of the test capsules were constructed as prototypes of the FFTF absorber pins, and loaded with absorber pellets representative of material termed FFTF reference boron carbide. For tests in EBR-II the boron was generally 92% enriched rather than natural boron as used in FFTF. As a result of this intensive test program, irradiation data were obtained for this reference material over the temperature range of 500°C to 1000°C up to burnup levels as high as 180×10^{20} captures/cm^3. Results have confirmed that the reference assembly will meet the design requirements for FFTF operations.

Longer absorber pin lifetimes, up to 3 years, are achieved by increasing the pellet-to-cladding gap from 0.014 inch to 0.045 inch and using a vented pin design which avoids pressure build-up in the pins from helium formed in the (n, α) reaction. Under such conditions the absorber duct could experience the highest fast neutron fluence of any core component: 3×10^{23} neutrons

per square centimeter. This causes duct bowing to be a second major lifetime limiting phenomenon for the absorber assemblies. The differential bowing between the inner, movable duct and the outer fixed duct determines the functional limitations on absorber duct lifetimes. The longer absorber assembly lifetimes are achieved by selecting an alloy for the structural material which has reduced swelling characteristics. In addition with the vented pin concept, the boron carbide pins and hence inner ducts can be made shorter because there is no need to provide space for gas plenum. The shorter lengths ameliorate bow of the inner duct.

Figure 40 shows the major secondary effort which was directed toward investigating alternate absorber materials. EBR-II irradiation of tantalum and europium sesquioxide was completed to moderate exposure levels (approximately 15×10^{20} captures/cm^3). Further development of these materials was discontinued based primarily on potential afterheating problems (Ta) and reactivity worth limitations (Eu_2O_3 and Ta). Europium hexaboride has been identified as a potentially promising absorber material with nuclear and material properties comparable to those of boron carbide and reactivity worth about 10% higher than boron carbide for the same volume of material.

Future Developments

The focus of the fuels and materials development activities for the LMFBR is now aimed at using FFTF as a test reactor to obtain data on full scale components under truly prototypic conditions. Many tests have already been fabricated and those which will be under irradiation in FFTF, by Cycle 1 this year are summarized in Figure 41. Figure 42 summarizes the thrust of the fuels and blanket development activities. In addition to evaluating FFTF driver fuel, the next stage of the program will concentrate on cladding breach criteria, providing fuel assemblies with increased burnup capability, and with design modifications amenable to rapid, low cost fabrication. Also to be addressed are tests of high breeding ratio oxide and carbide fuels for future LMFBR's. Since the LMFBR basic designs are now aimed at heterogeneous

core designs to reduce sodium void coefficients, an activity is being started to develop and proof test internal blanket designs. Most of the new design concepts will utilize advanced alloy cladding and ducts. Data are already coming in from this phase of the program as for example in Figure 43, which is early data from one of the instrumented fuels tests now in FFTF.

Figure 44 summarizes the thrust of the absorber development program; in parallel with the fuel program, next activities will concentrate on evaluating the performance of the reference control rods for FFTF and on determining performance limits. Simultaneously, tests with large diameter vented pins using advanced alloy cladding and ducts in the assemblies, will be placed underway with the objective of achieving higher lifetimes and reduced costs. The first instrumented absorber test is also operating in FFTF, Figure 45.

The development program for cladding and duct materials will emphasize in-reactor performance tests in FFTF aimed at stress rupture, creep, and swelling properties and will continue work on four major classes of stainless steel as indicated in Figure 46. The bulk of the in-reactor testing will be done in the materials open test assembly or MOTA, for which a test train assembly is described in Figure 47. Development activities for the low swelling martensitic and ferritic materials will focus on fabricability and fracture toughness.

These experimental activities will continue to be supplemented by a complementary program of postirradiation examinations and continued improvement to design codes and design criteria. By the end of this decade LMFBR core components should reliably achieve useful lifetimes 2 to 3 times greater than those of today's FFTF components.

FUELS AND MATERIALS FOR LMFBR'S

C. M. COX
J. L. STRAALSUND
R. J. JACKSON

HANFORD ENGINEERING DEVELOPMENT LABORATORY

DEVELOPMENT PROGRAM

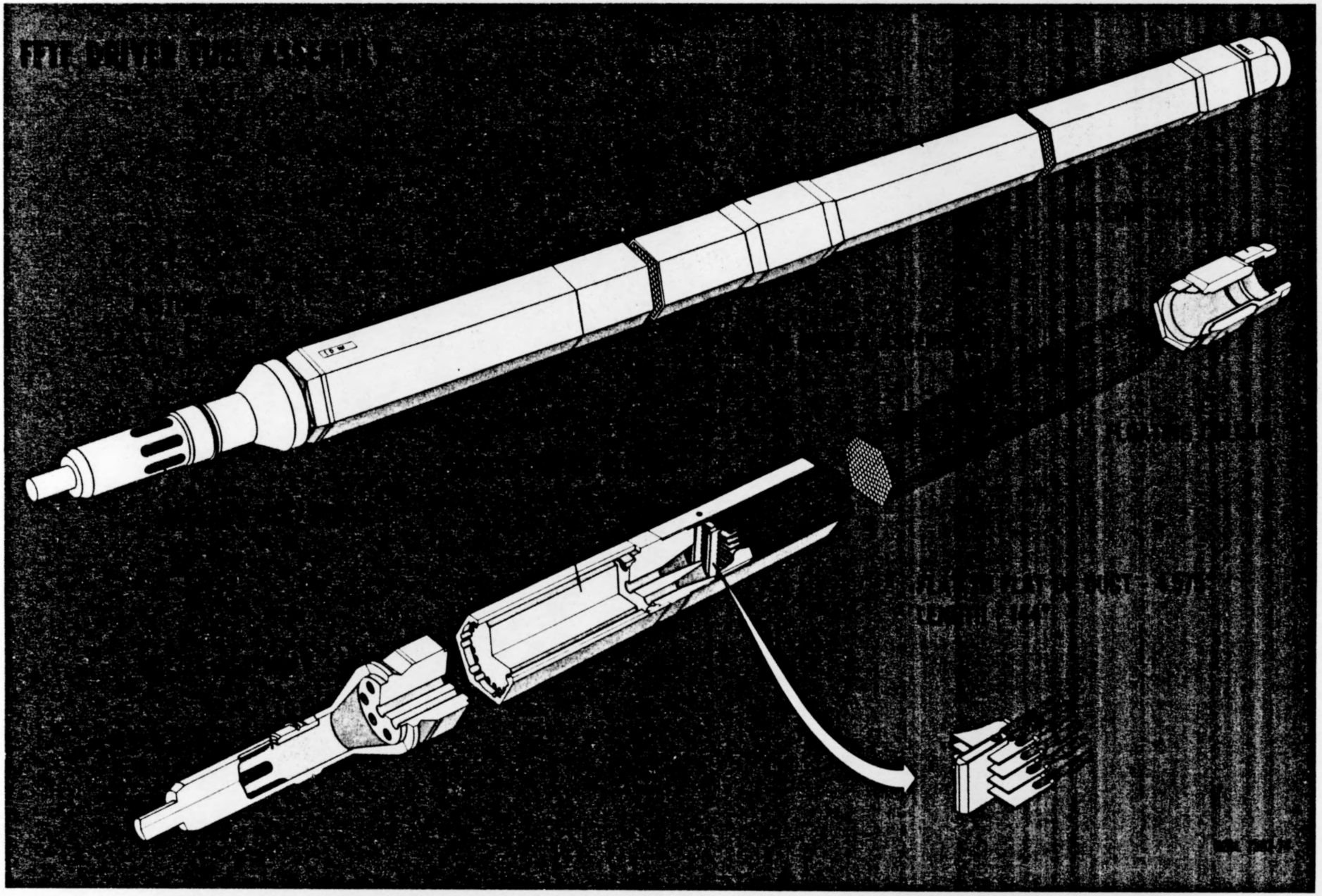

FIGURE 1, FFTF DRIVER FUEL ASSEMBLY

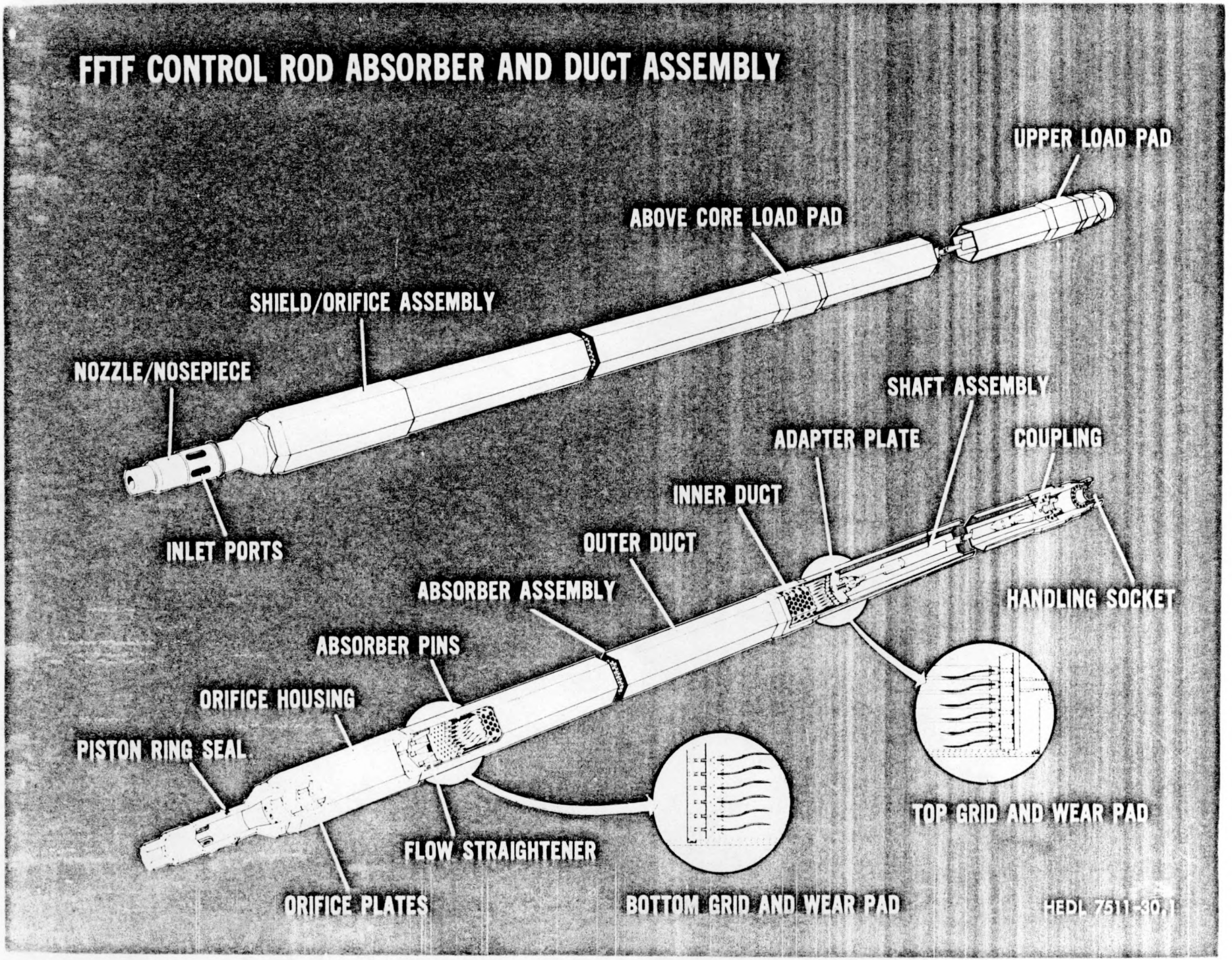

FIGURE 2, FFTF CONTROL ROD ABSORBER AND DUCT ASSEMBLY

COMPARISON OF LMFBR FUEL ASSEMBLIES

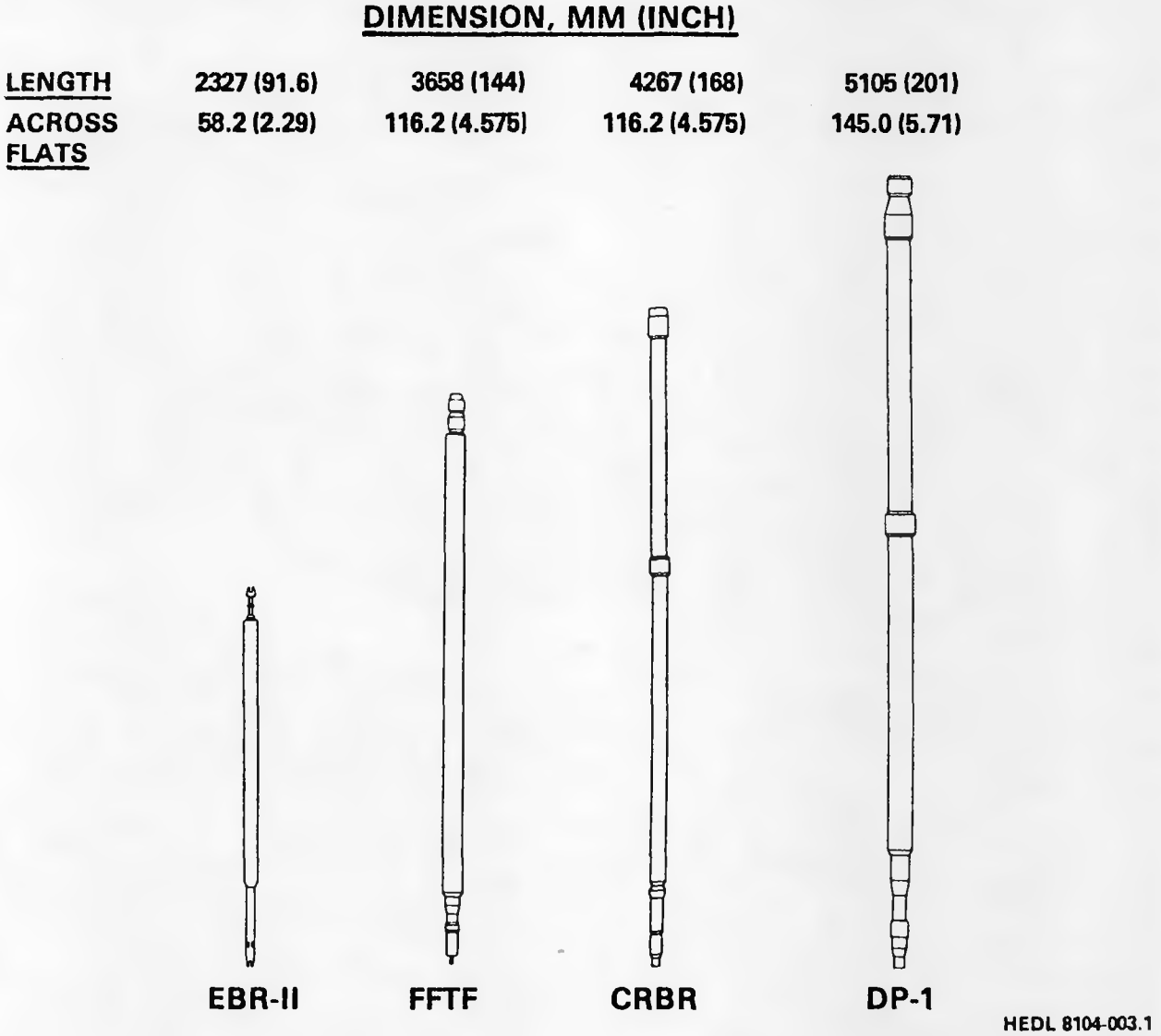

FIGURE 3, COMPARISON OF LMFBR FUEL ASSEMBLIES

SCOPE OF IRRADIATION PROGRAMS IN EBR-II

FUELS	BLANKETS	ABSORBER	STAINLESS STEELS
$(U,Pu)O_2$	UO_2	B_4C	AUSTENITIC
(U,Pu)C	UC	$B_{6.5}C$	MARTENSITIC
(U,Pu)N	ThO_2	EuB_6	FERRITIC
$(Pu,Th)O_2$		Eu_2O_3	PRECIPITATION STRENGTHENED
(Pu,Th)C		Ta	

FIGURE 4, SCOPE OF IRRADIATION PROGRAMS IN EBR-II

MIXED OXIDE IRRADIATIONS

(PNL-9,10,11 EBR II B-61-A S/A)

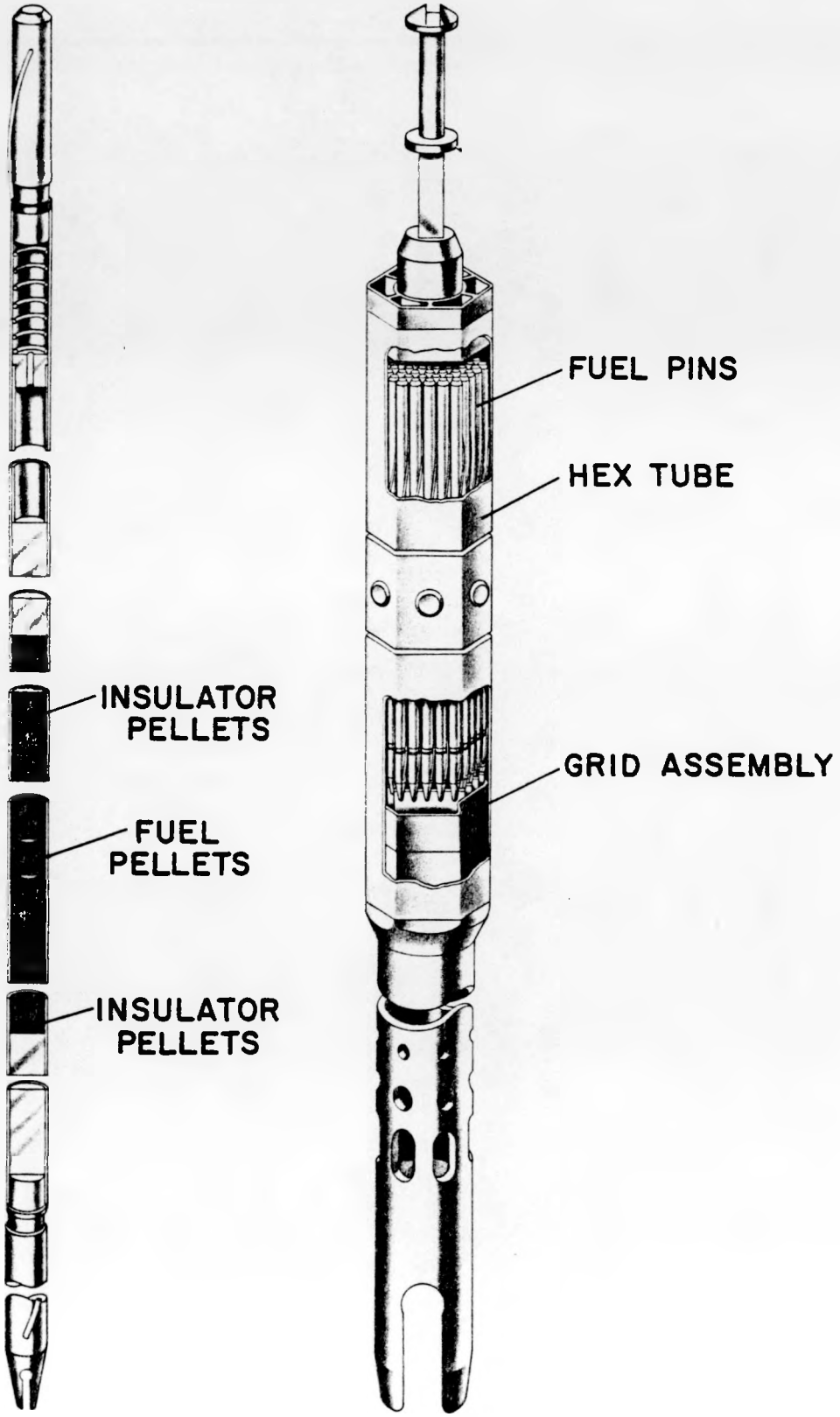

FIGURE 5, MIXED OXIDE IRRADIATIONS

TRANSIENT TESTS OF MIXED OXIDE FUEL PINS

PIN TYPES	NUMBER OF PINS OR TESTS		
	TREAT CAPSULE TESTS	TREAT LOOP TESTS	POSTIRRADIATION CLADDING TRANSIENT TESTS
$(U,Pu)O_2$	48	50	300
(U,Pu)C	13	7	0

FIGURE 6, TRANSIENT TESTS OF MIXED OXIDE FUEL PINS

HEDL MARK III TREAT SODIUM TEST LOOP

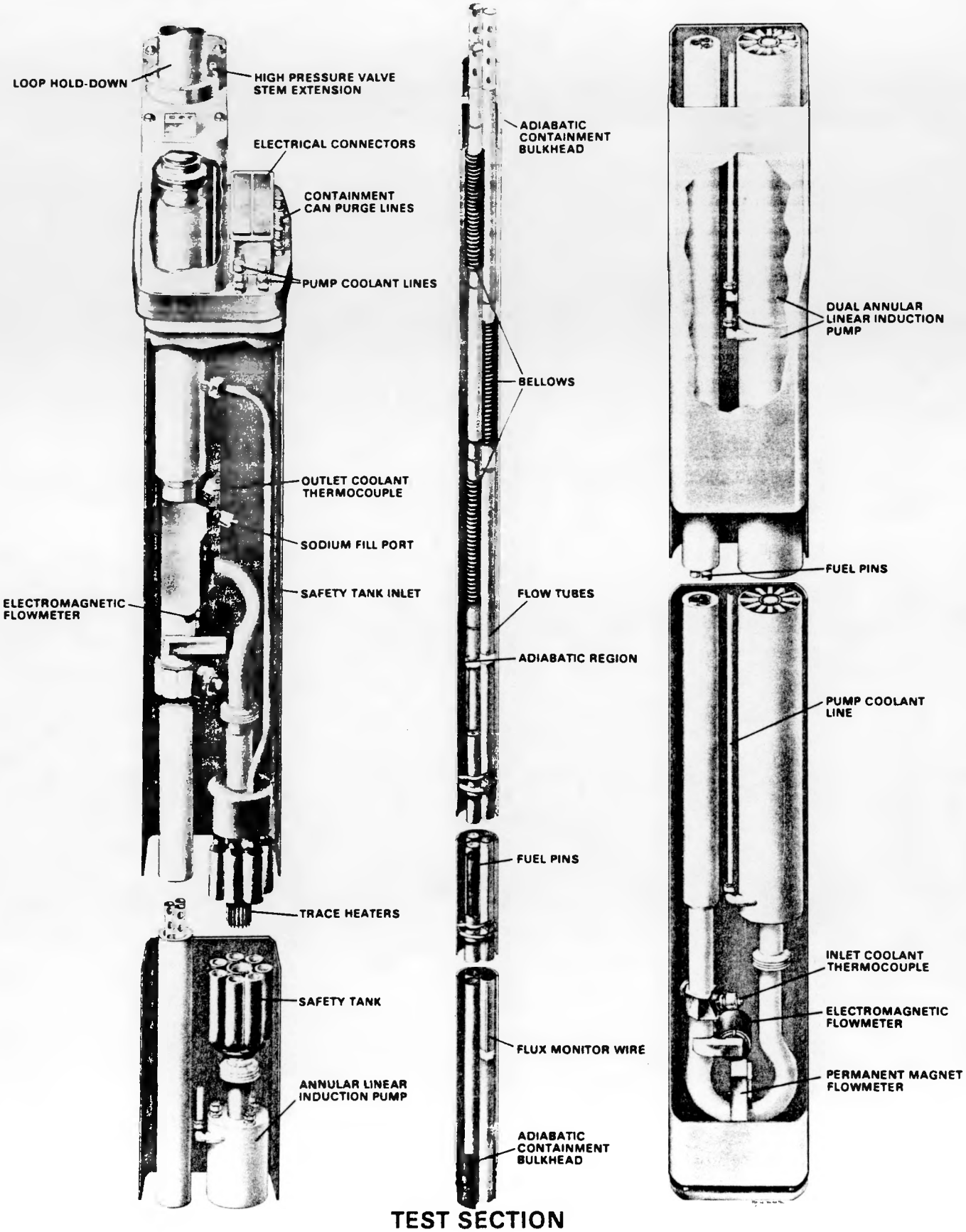

FIGURE 7, HEDL MARK III TREAT SODIUM TEST LOOP

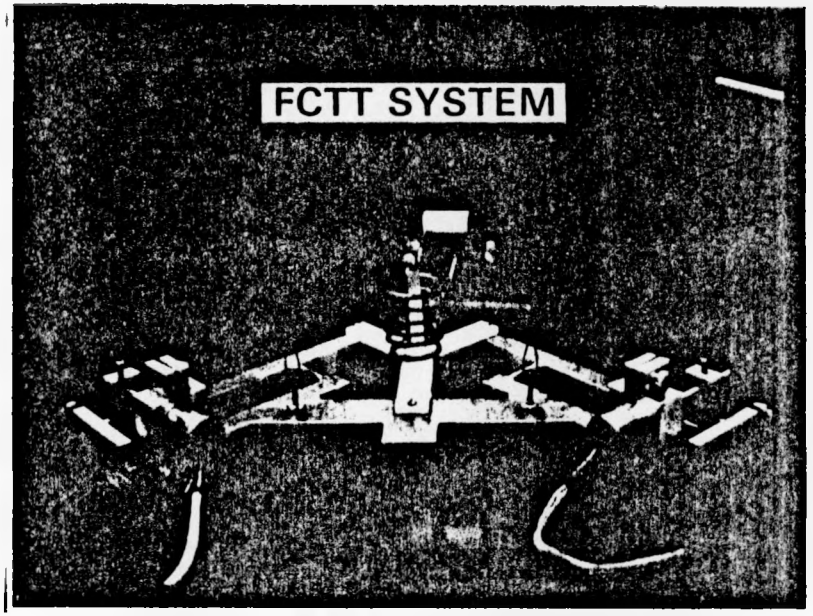

FIGURE 8, FUEL-CLADDING TRANSIENT TEST SYSTEM

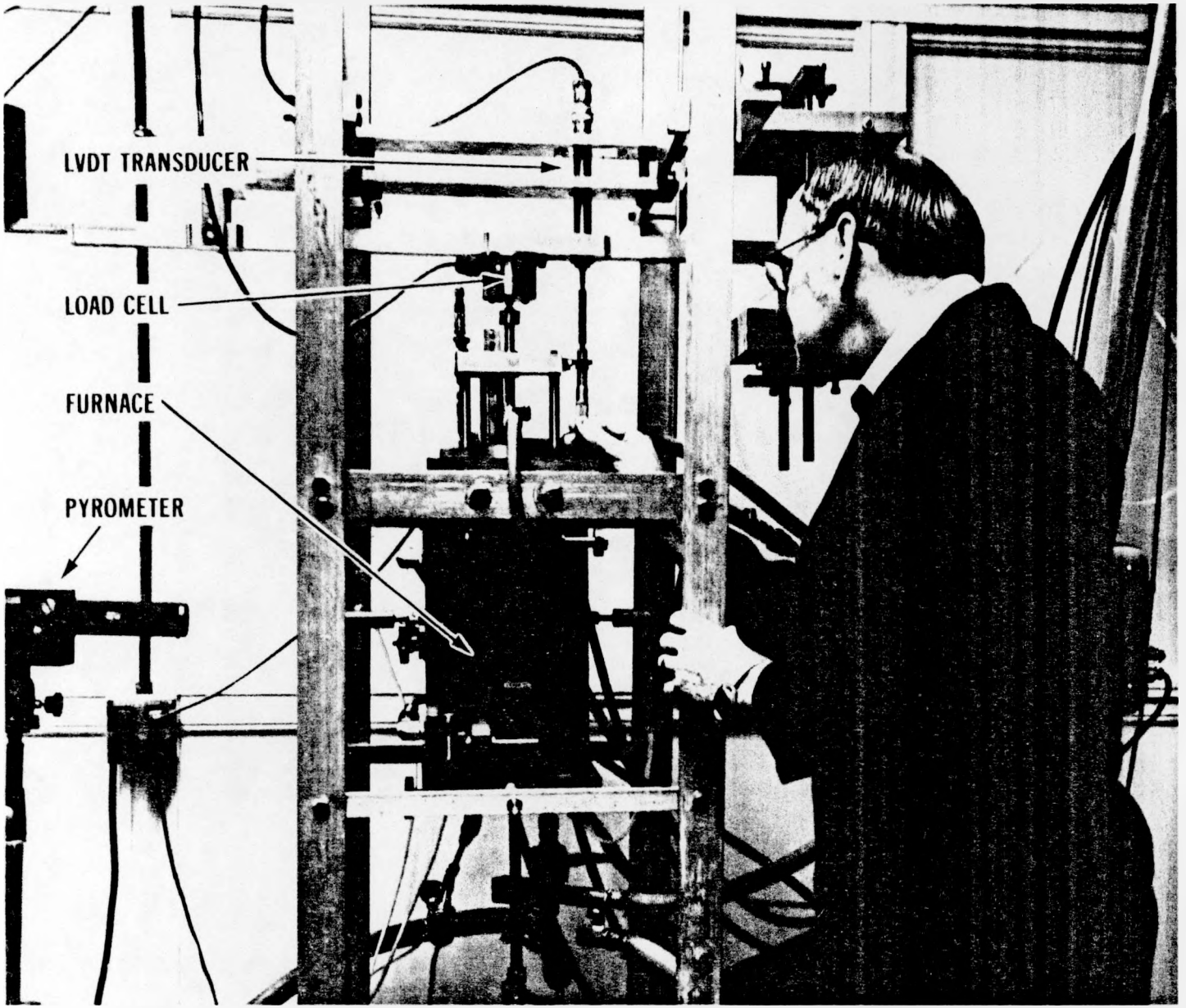

FIGURE 9, HIGH TEMPERATURE CREEP SYSTEM (T>2000°C)

TEMPERATURE AND POWER DISTRIBUTION

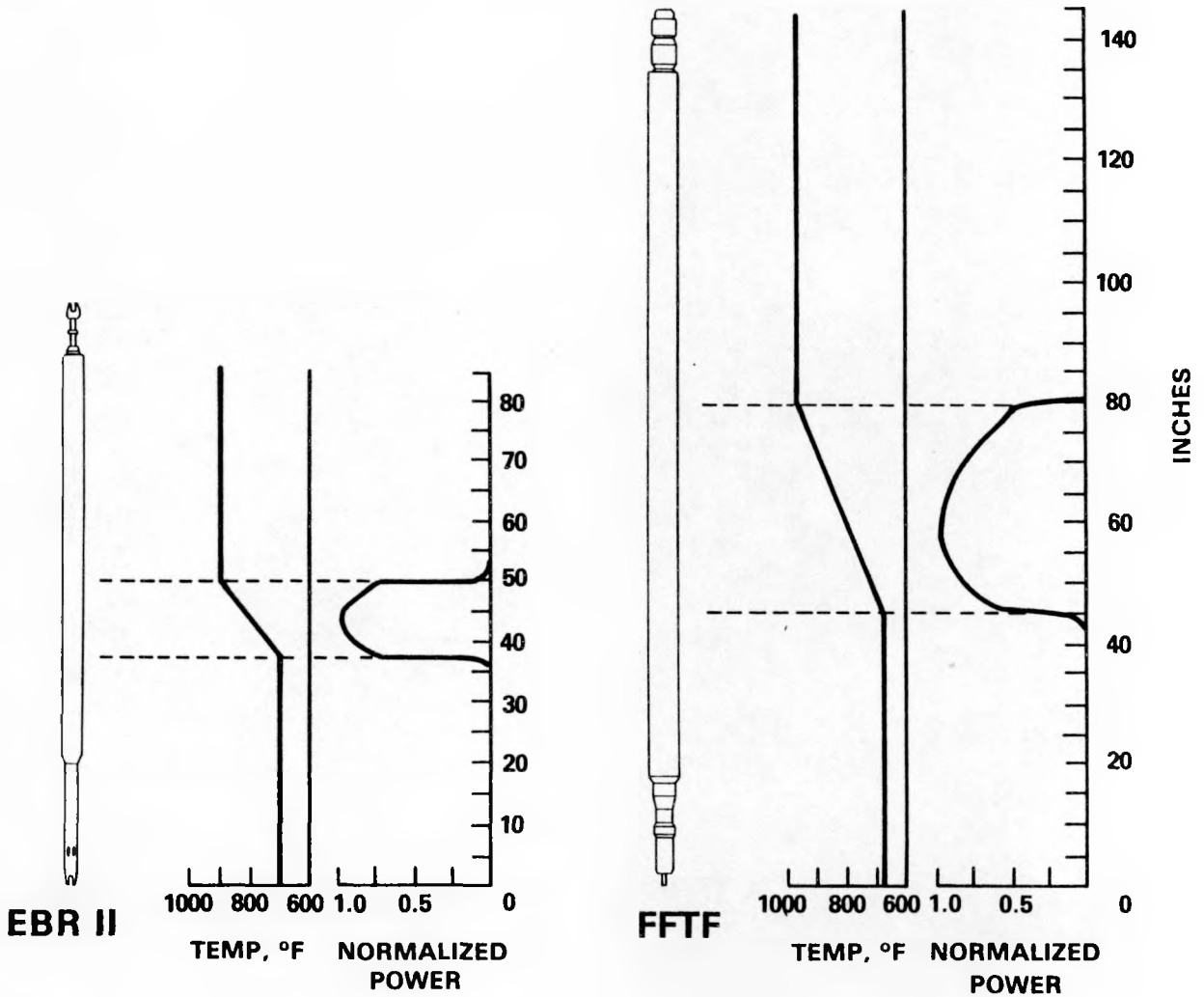

FIGURE 10, TEMPERATURE AND POWER DISTRIBUTION

TYPICAL INSTRUMENTED FUEL ASSEMBLY

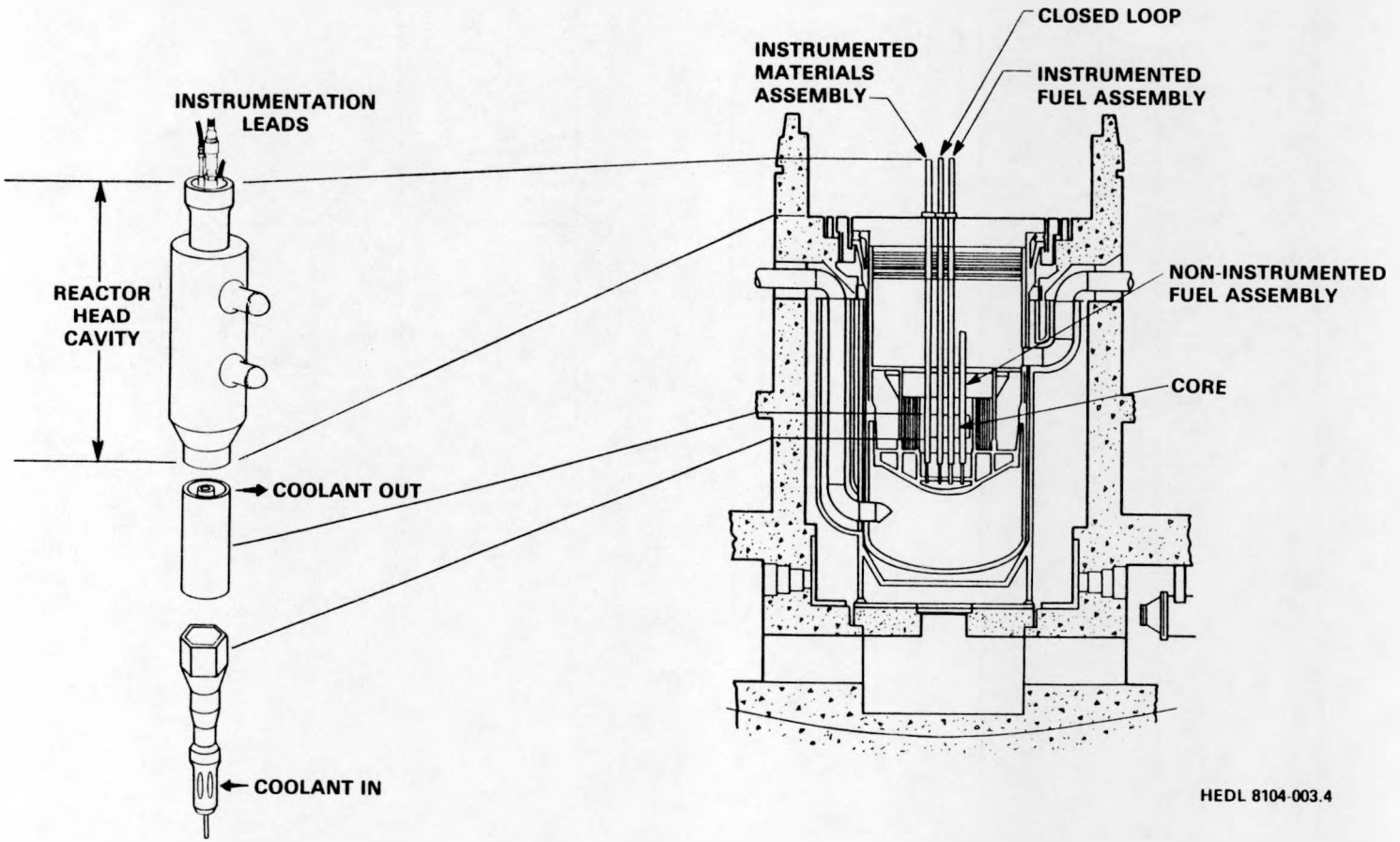

FIGURE 11, TYPICAL INSTRUMENTED FUEL ASSEMBLY

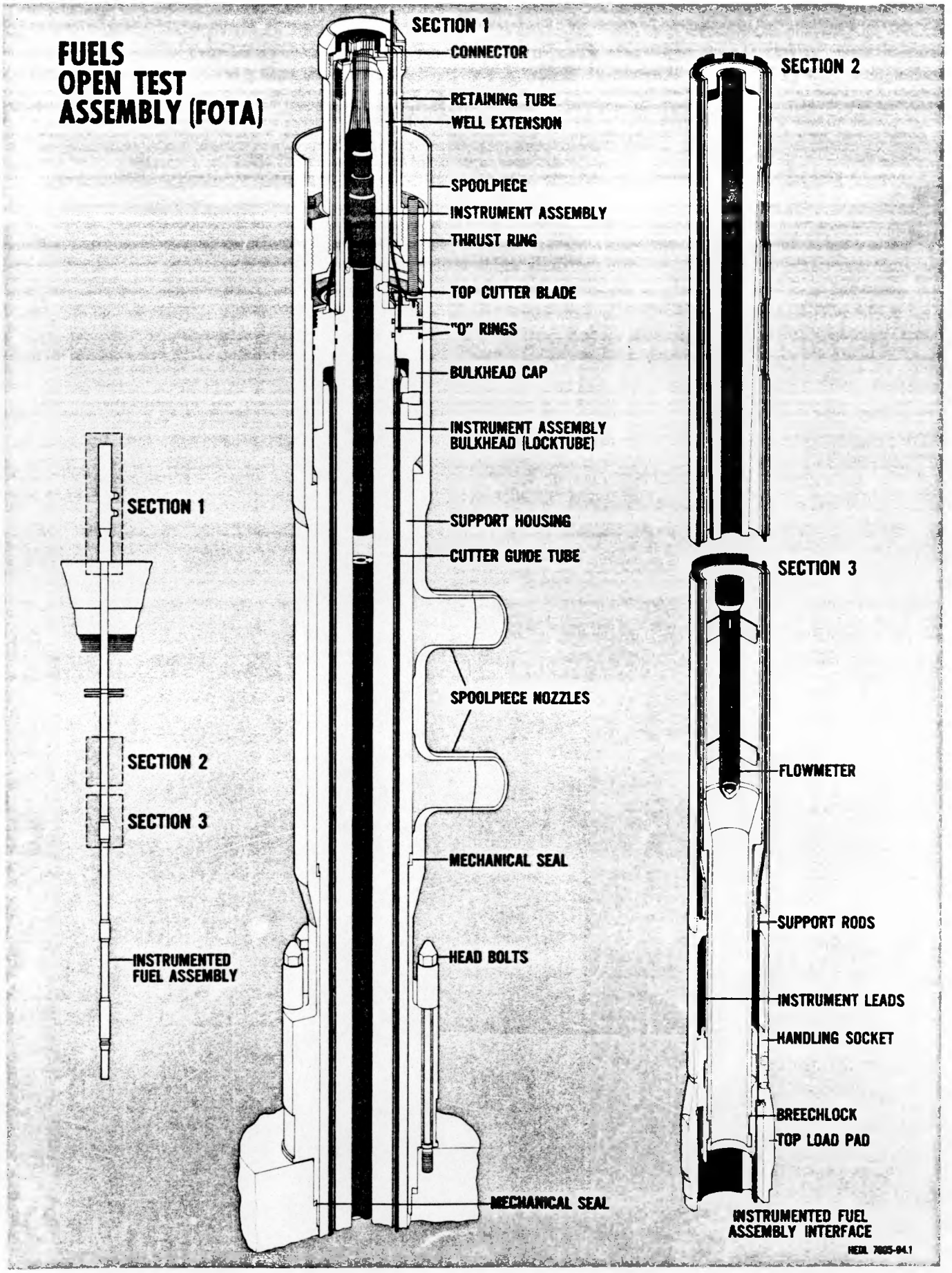

FIGURE 12, FUELS OPEN TEST ASSEMBLY (FOTA)

DUCTS

FFTF CORE ENVIRONMENT

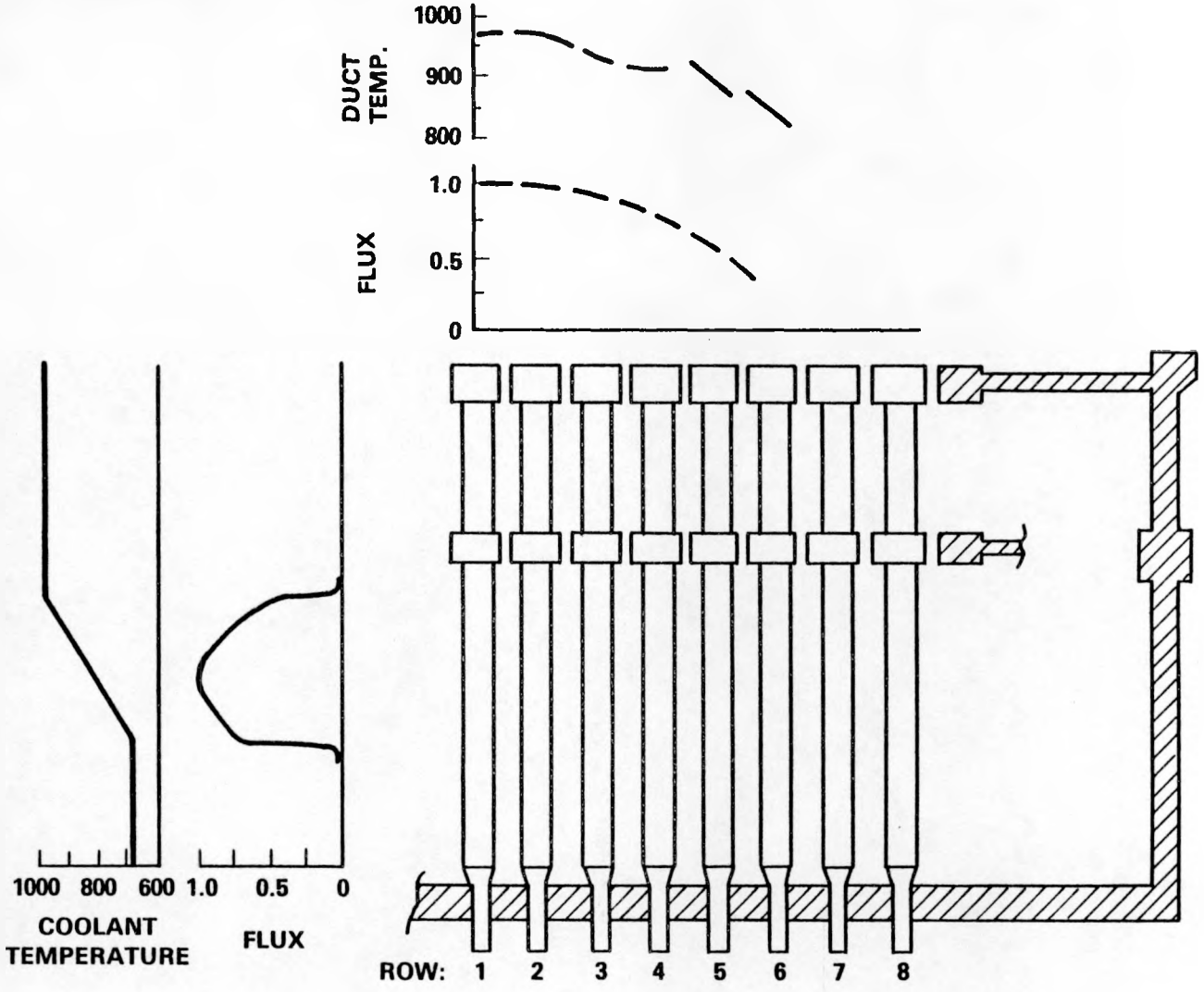

FIGURE 13, FFTF CORE ENVIRONMENT

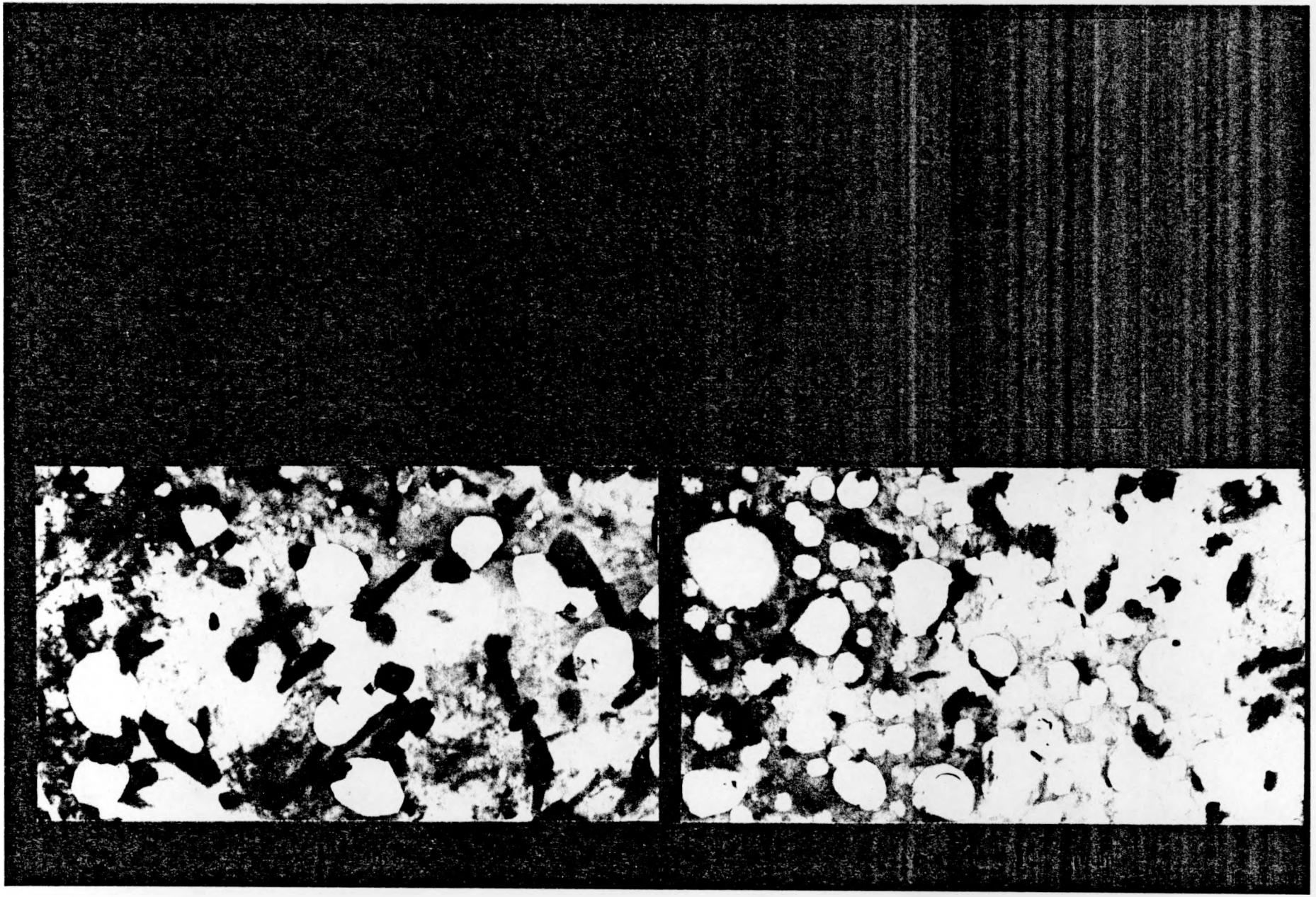

FIGURE 14, EFFECT OF FLUENCE ON CLADDING SWELLING

20% CW 316
PNL -11-9R

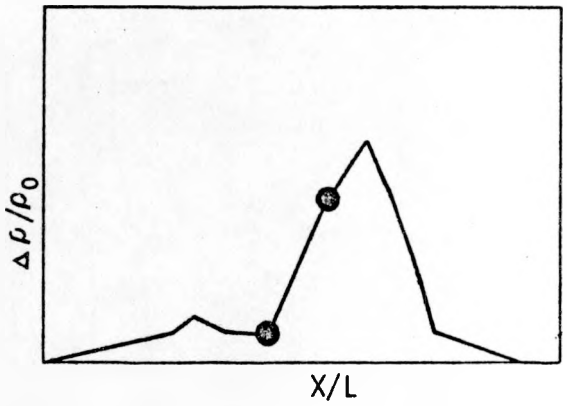

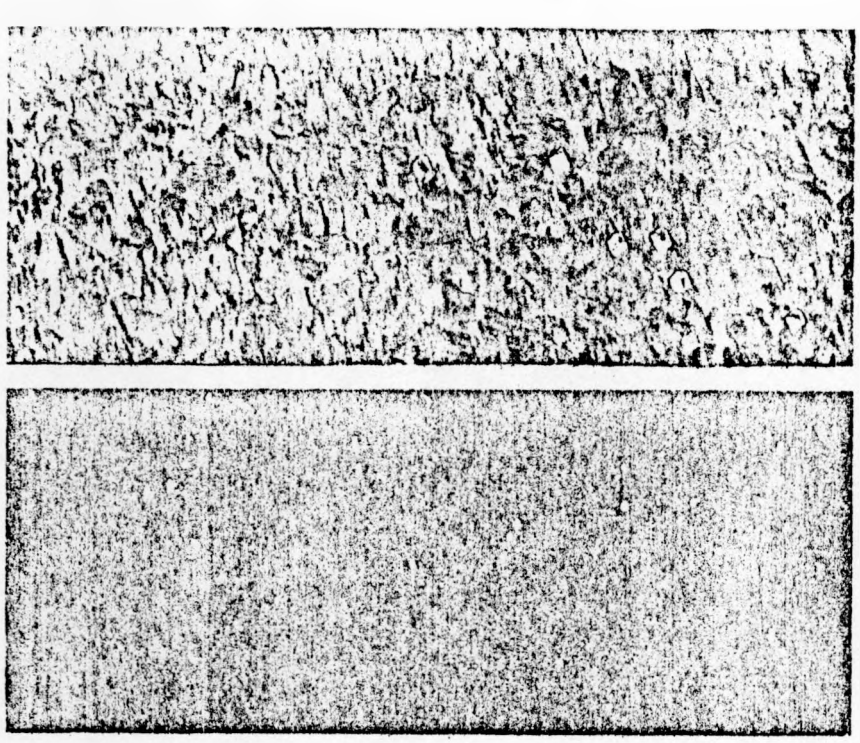

2770 4498

$\Phi t \sim 9.8 \times 10^{22}$ n/cm^2 T ~ 455°C

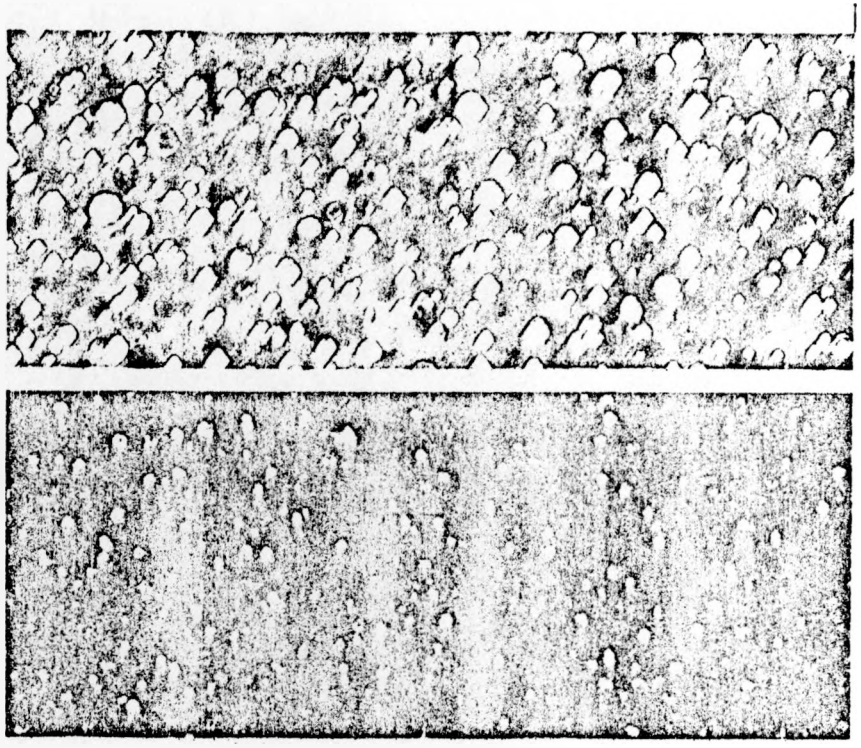

2741 6264

$\Phi t \sim 10.0 \times 10^{22}$ n/cm^2 T ~ 480°C

HEDL 7806-148.10

FIGURE 15, TEMPERATURE EFFECTS ON CLADDING SWELLING

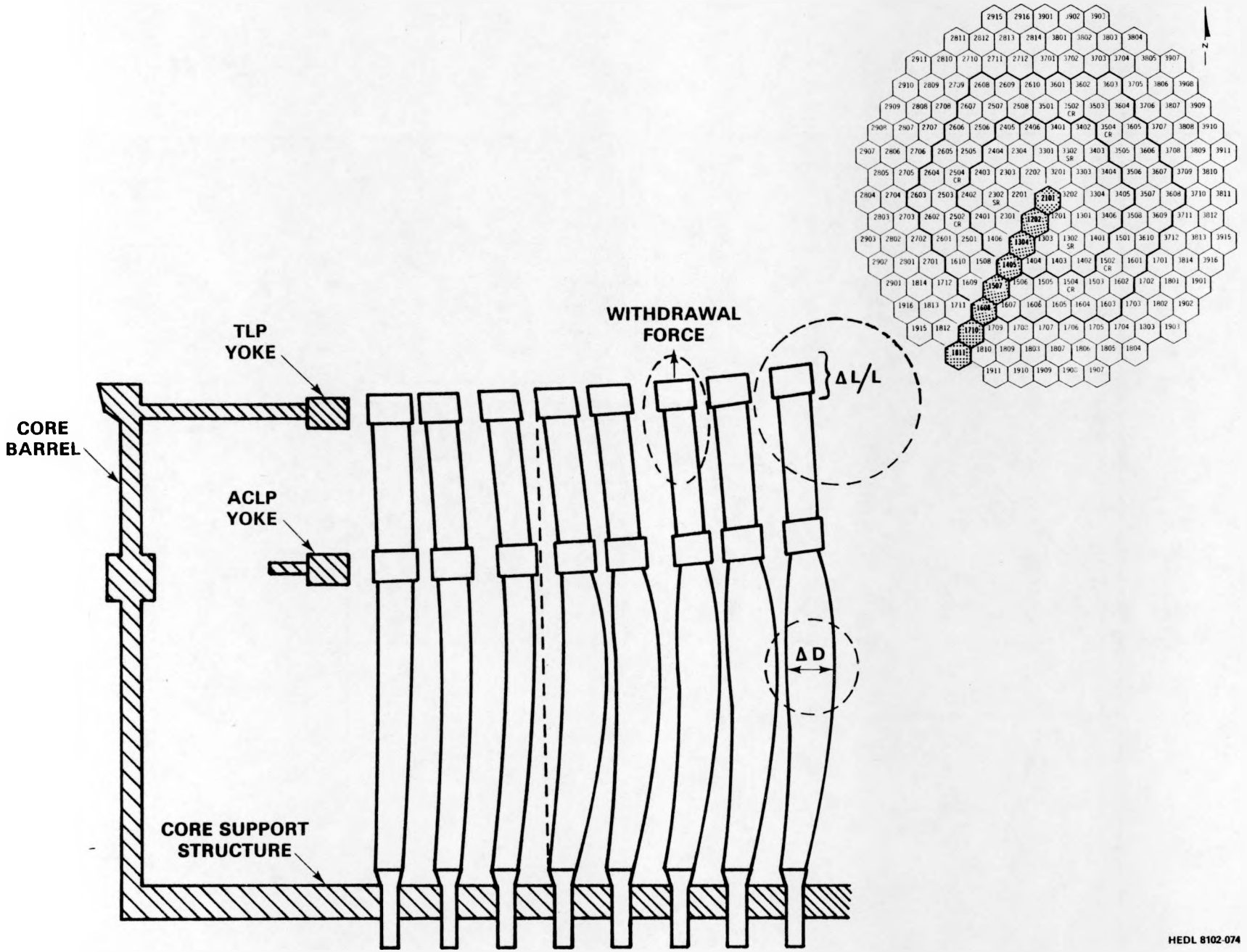

FIGURE 16, DUCT LIFETIME CRITERIA

COMPARISON OF THERMAL AND IRRADIATION CREEP

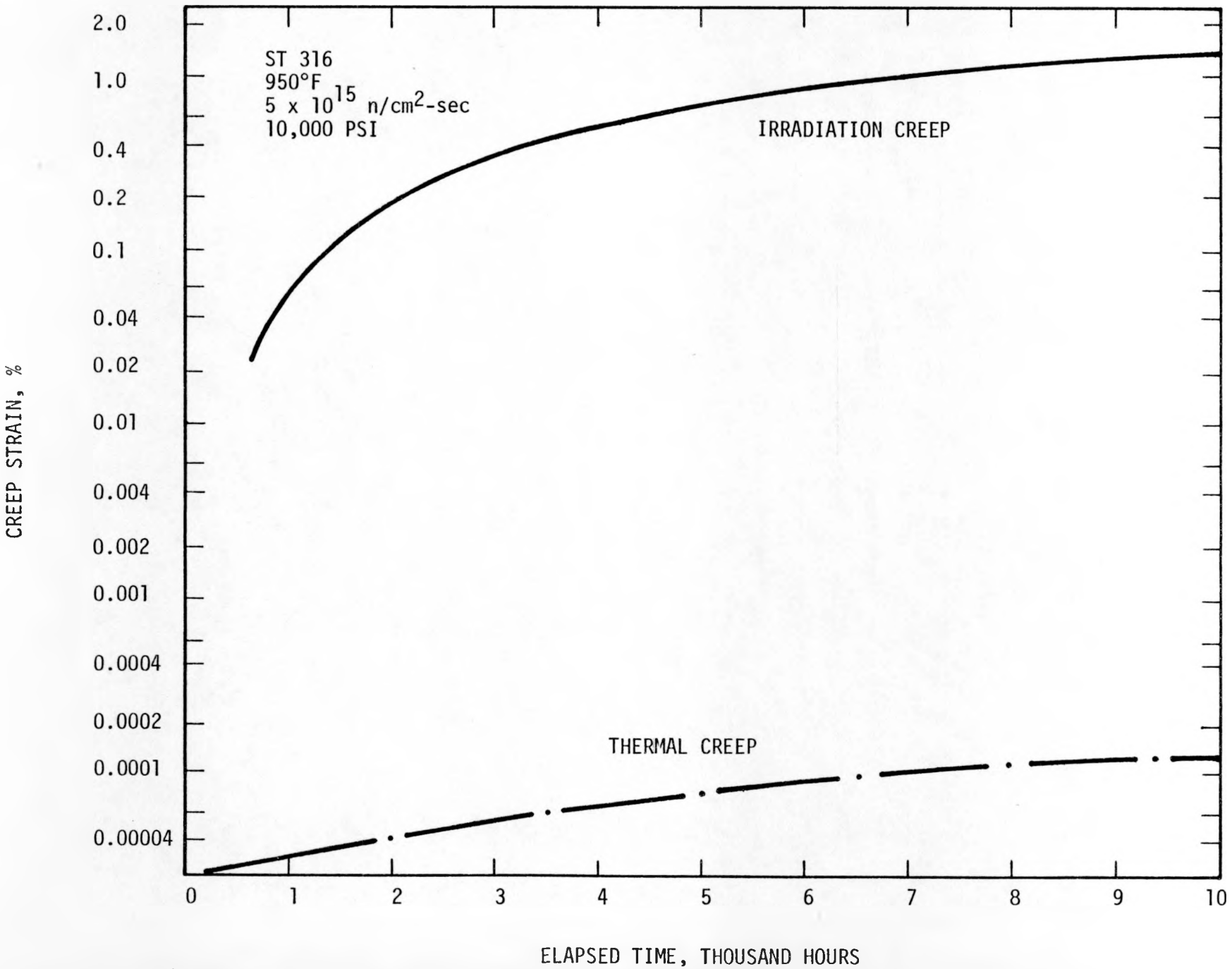

FIGURE 17, COMPARISON OF THERMAL AND IRRADIATION CREEP

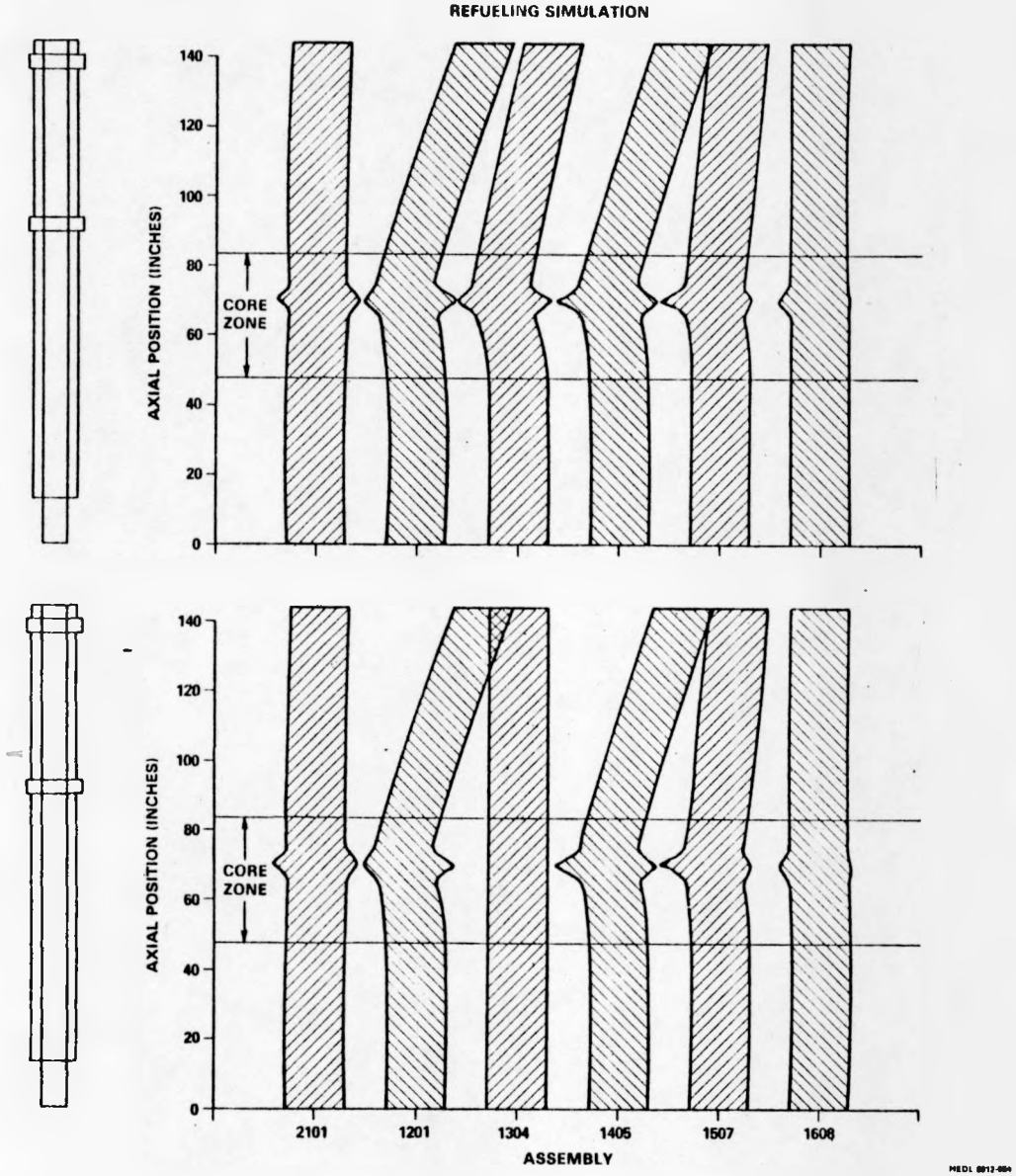

FIGURE 18, REFUELING SIMULATION WITH NEW ASSEMBLY IN ROW 3

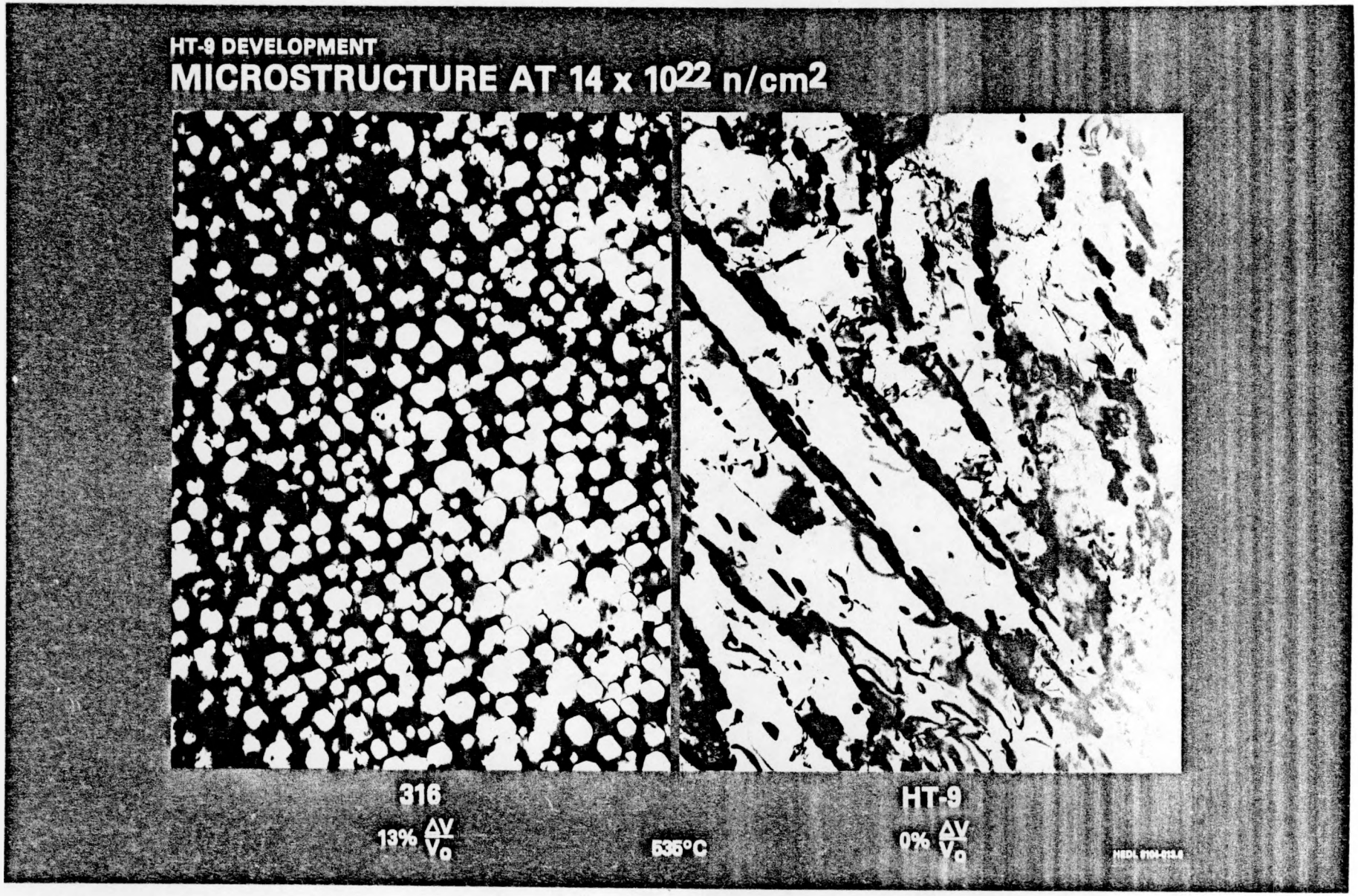

FIGURE 20, MICROSTRUCTURE AT 14 x 10^{22} n/cm^2

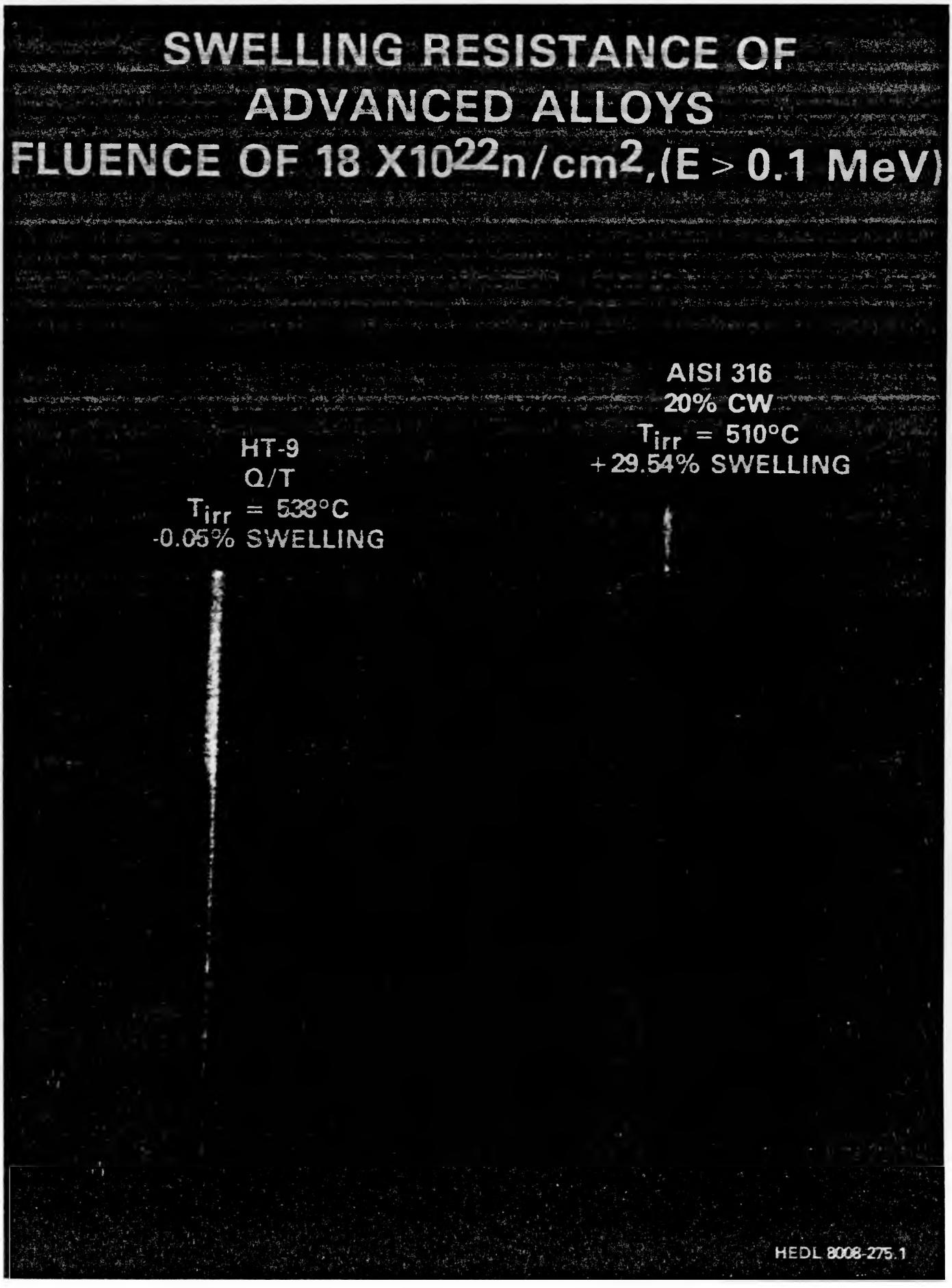

FIGURE 19, SWELLING RESISTANCE OF ADVANCED ALLOYS FLUENCE OF 18x10^{22}n/cm^2,(E>0.1 MeV)

CALCULATED DUCT DISTORTION

FFTF RADIAL ROW DURING REFUELING AFTER 400 DAYS

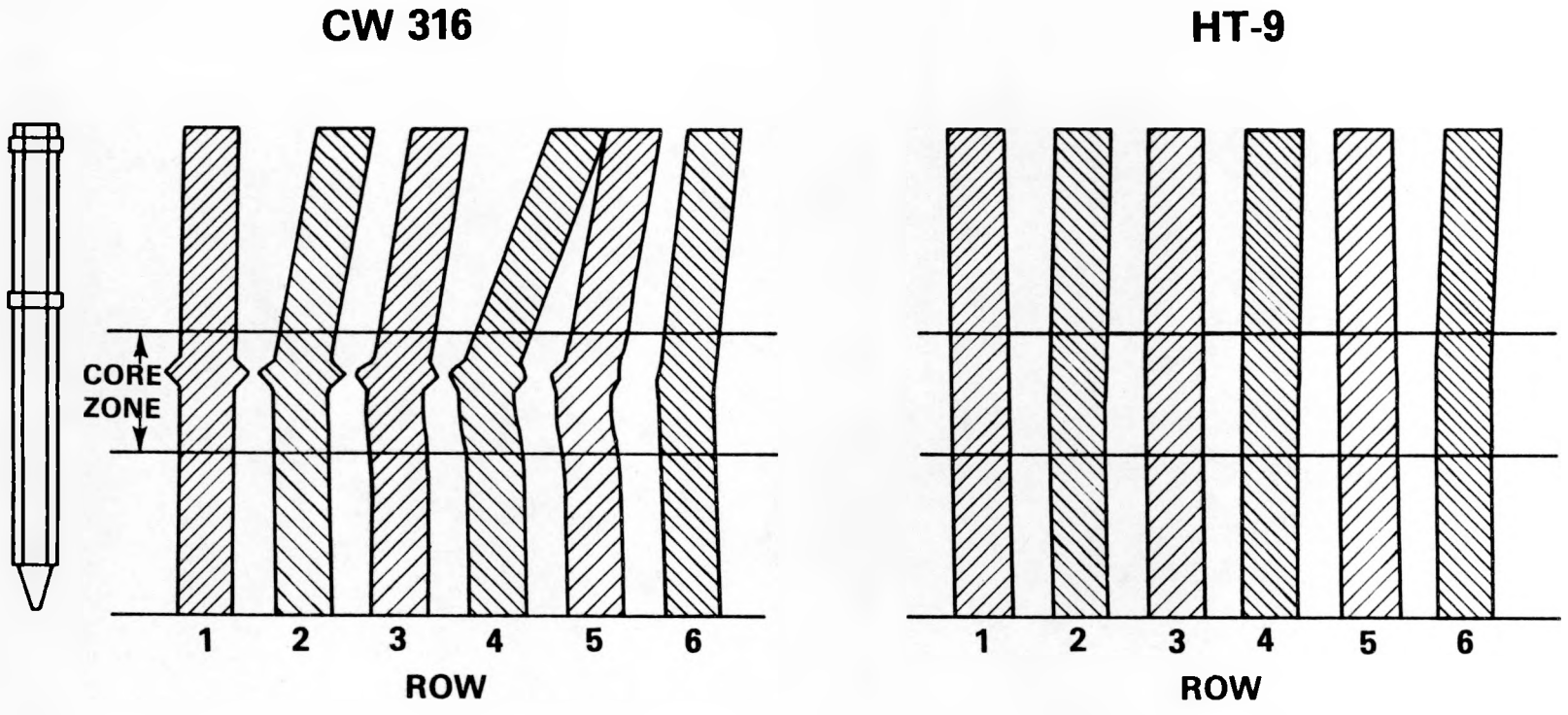

FIGURE 21, CALCULATED DUCT DISTORTION

FUEL PINS

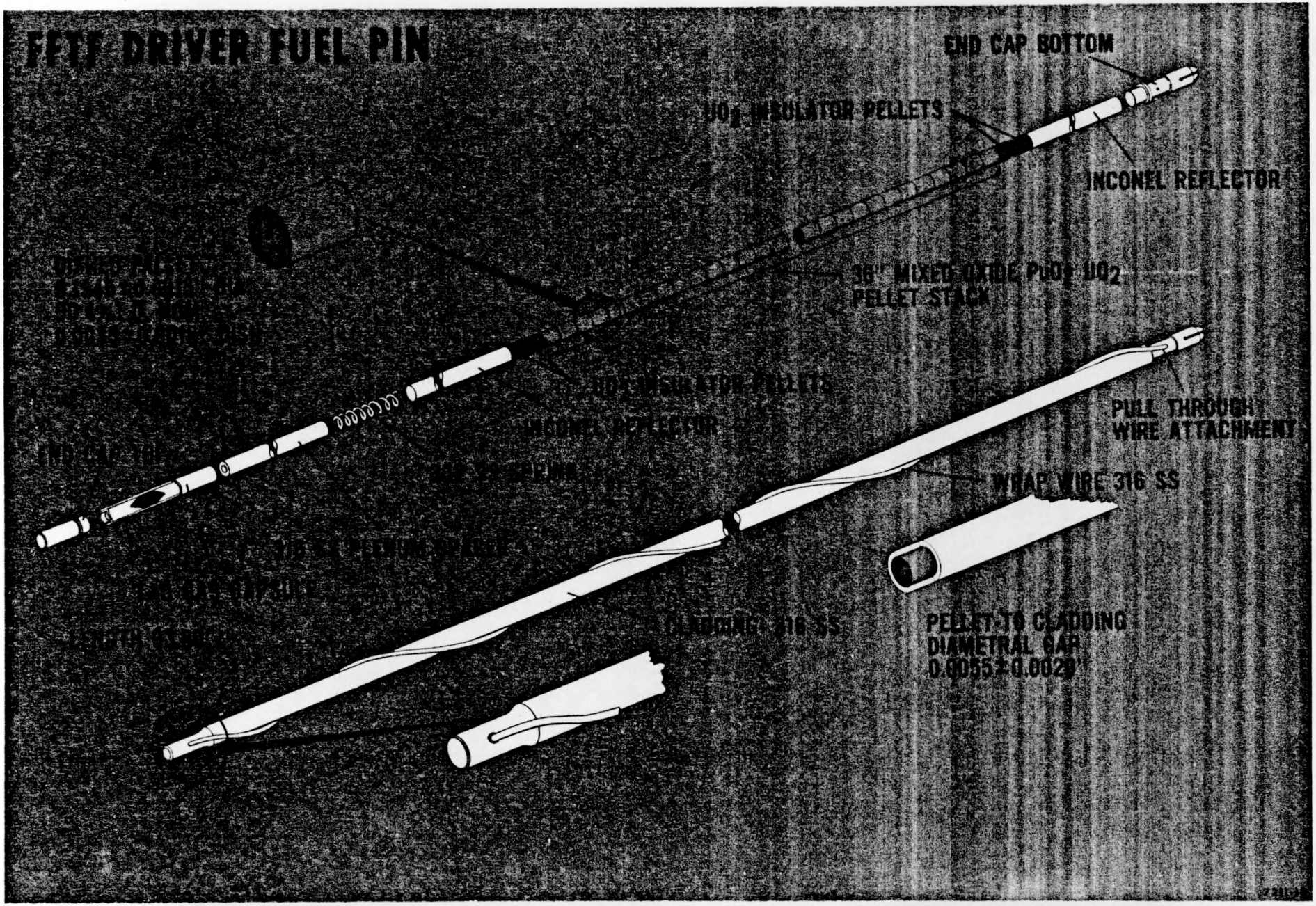

FIGURE 22, FFTF DRIVER FUEL PIN

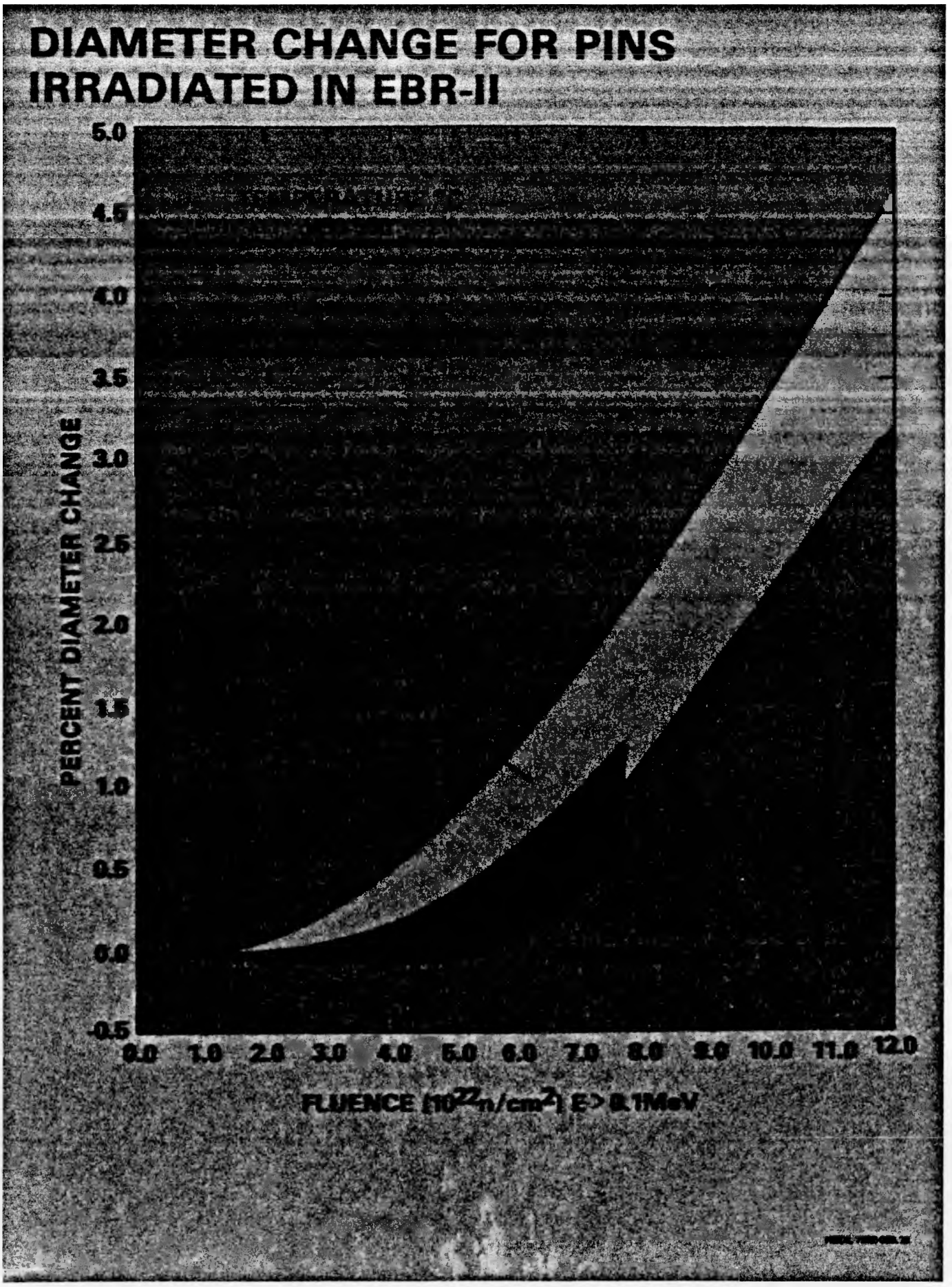

FIGURE 23, DIAMETER CHANGE FOR PINS IRRADIATED IN EBR-II

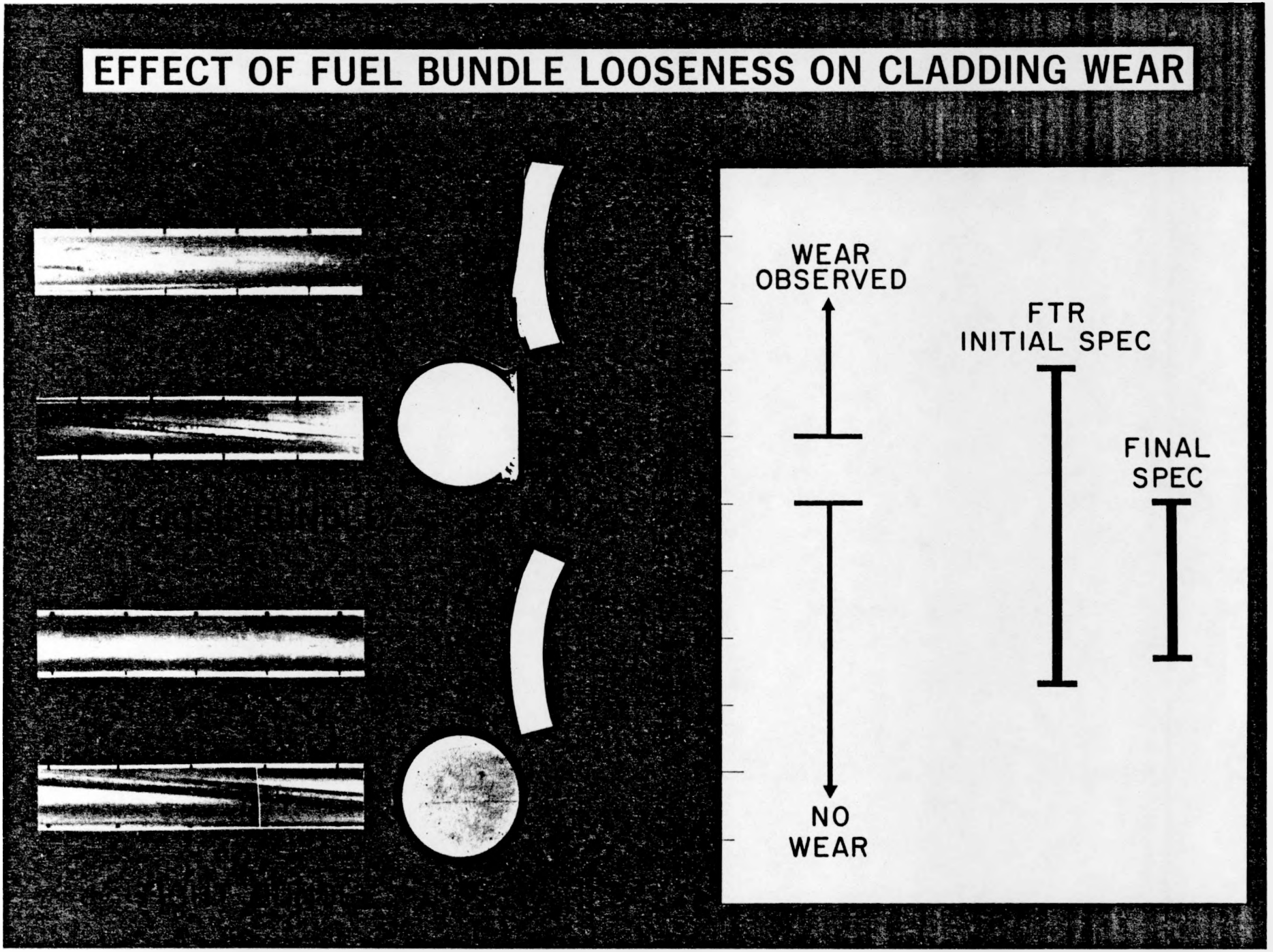

FIGURE 24, EFFECT OF FUEL BUNDLE LOOSENESS ON CLADDING WEAR

FUEL RESTRUCTURING

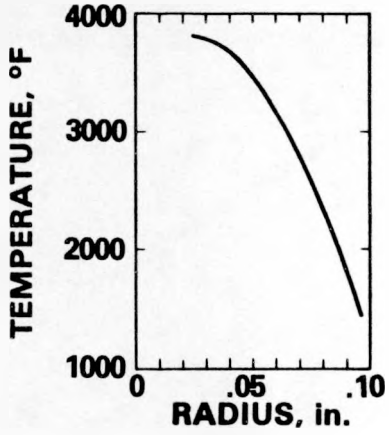

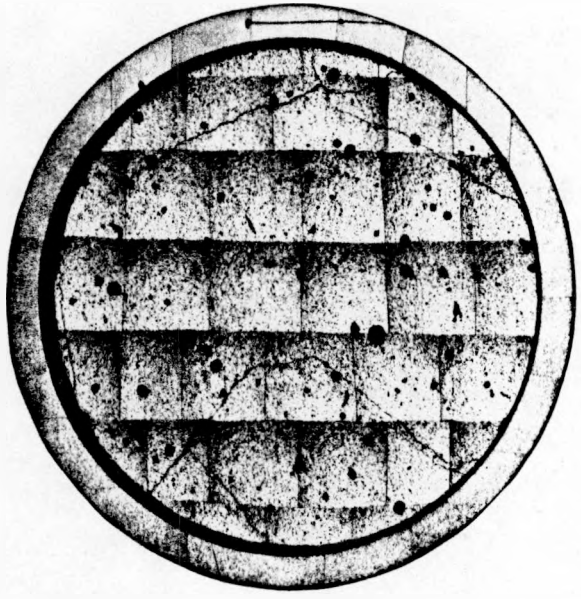

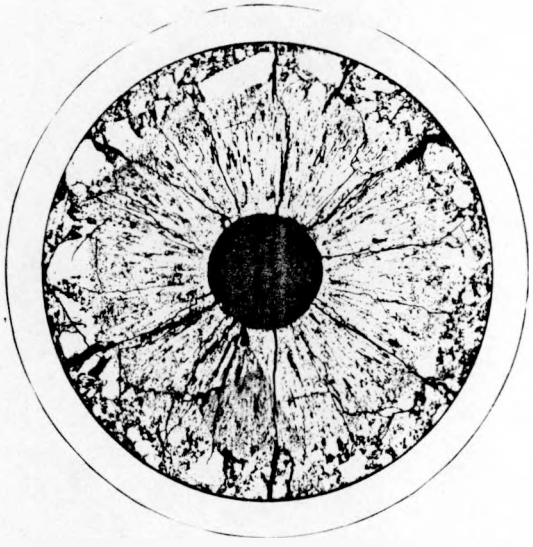

AS FABRICATED

IRRADIATED

HEDL 8104-116.2

FIGURE 25, FUEL RESTRUCTURING

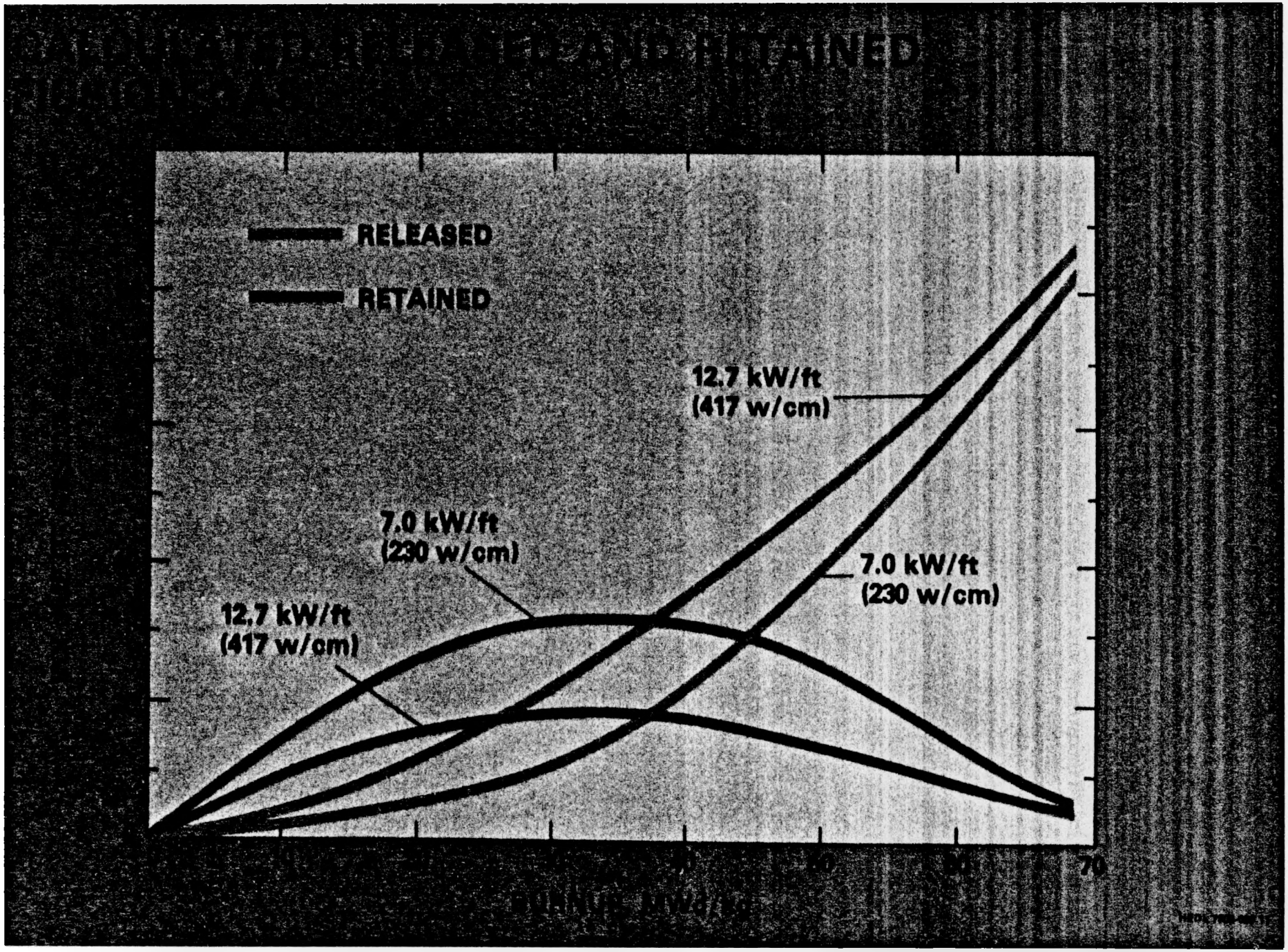

FIGURE 26, CALCULATED RELEASED AND RETAINED FISSION GAS

FUEL-CLADDING CHEMICAL INTERACTION

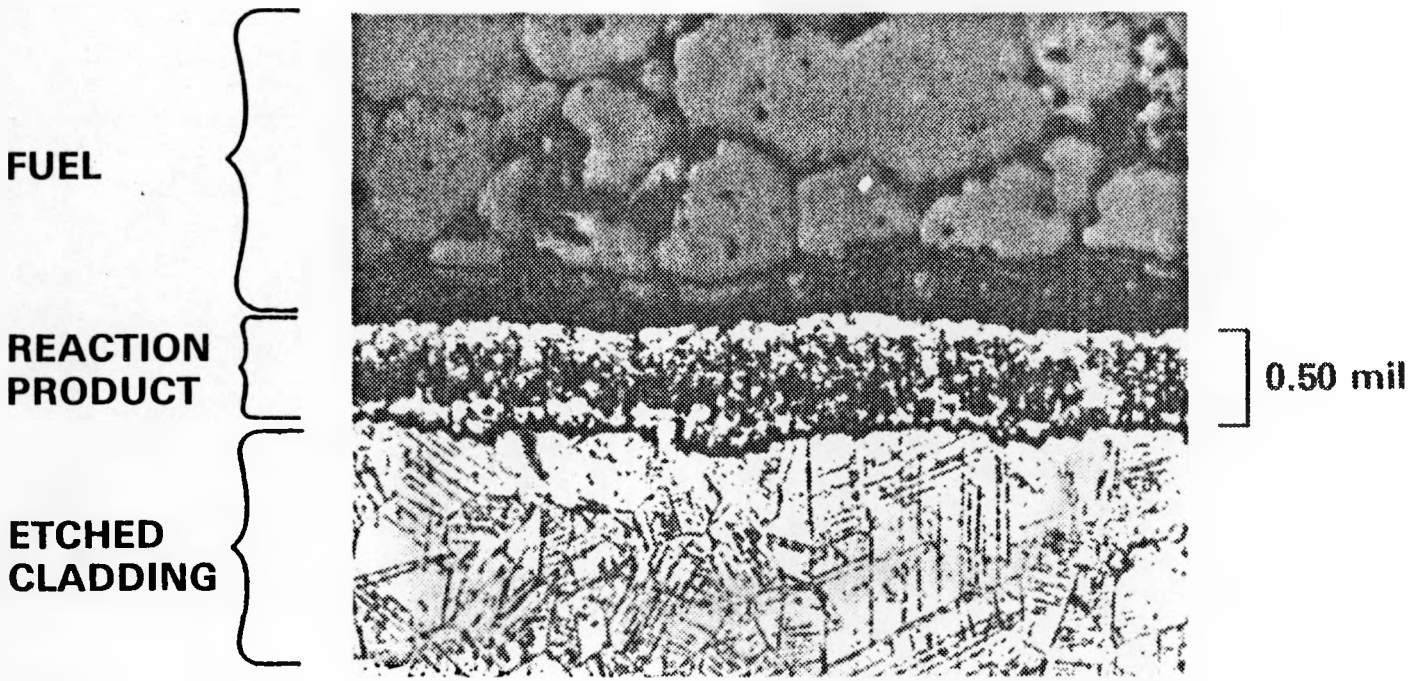

FIGURE 27, FUEL-CLADDING CHEMICAL INTERACTION

FIGURE 28, Axial Extent of Melting with Respect to the Central Void (P-19-27R, Sample H-1).

Photo No. 775869-1

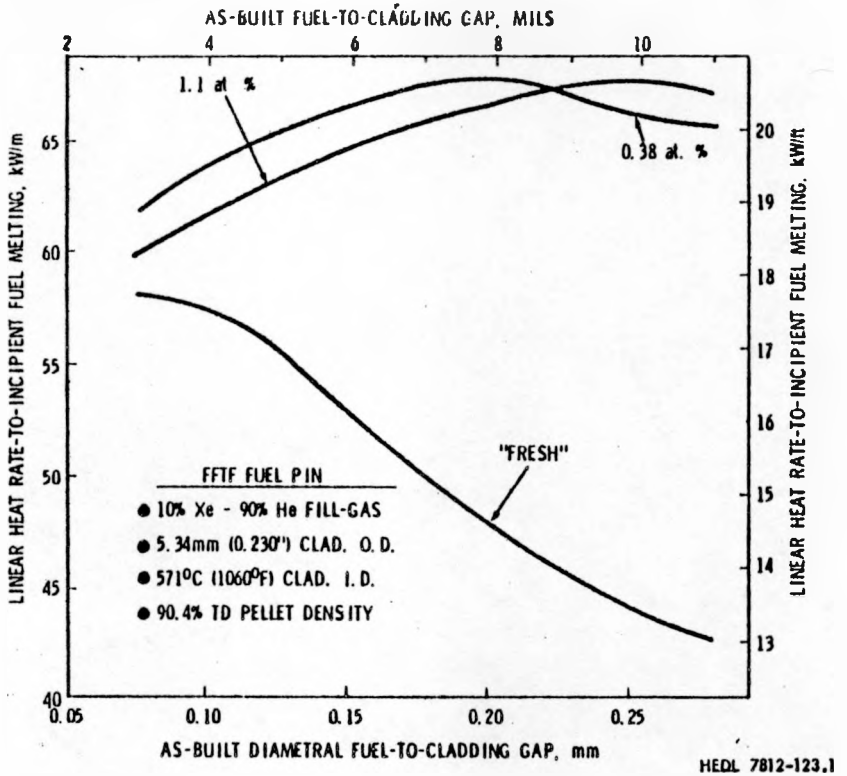

FIGURE 29, PREDICTIONS OF Q'_m FOR FFTF DRIVER FUEL PINS

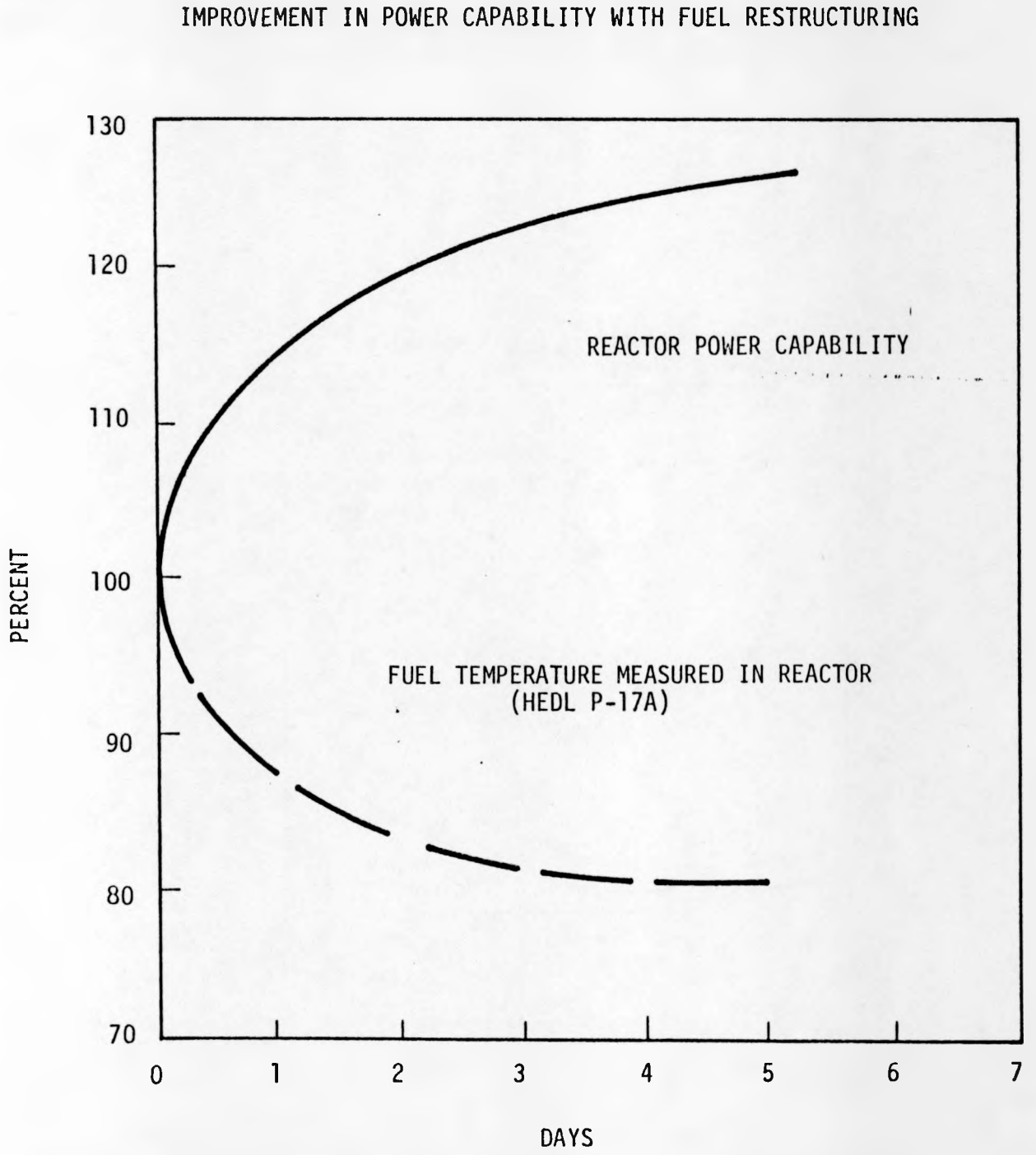

FIGURE 30, IMPROVEMENT IN POWER CAPABILITY WITH FUEL RESTRUCTURING

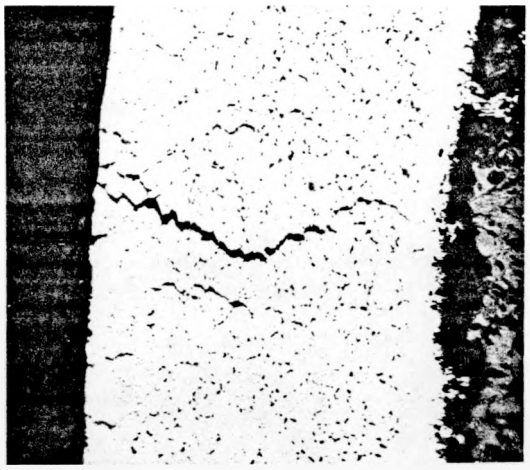

a) The Breach Area Etched to Show Intermetallic Precipitates

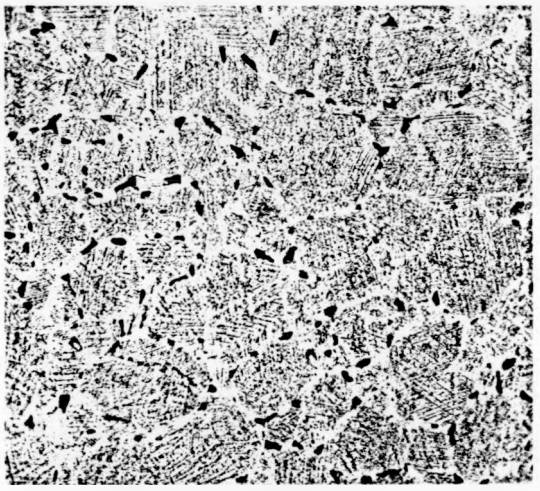

b) Microstructure Near The Cladding Breach

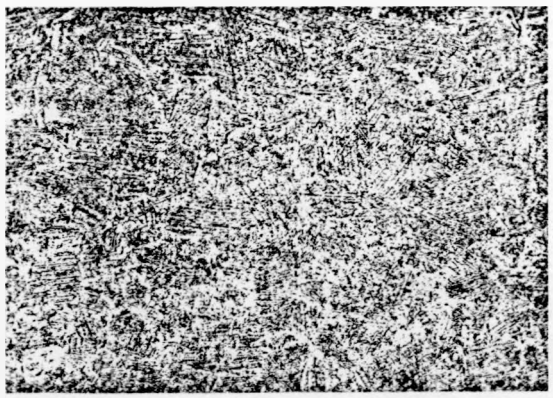

c) Cladding Microstructure 90 Degrees From Breach Site

HEDL 7908-208.3

FIGURE 31, EXAMPLE OF MICROSTRUCTURE DIFFERENCES NEAR A CLADDING HOT SPOT AND REMOVED FROM THE HOT SPOT

HIGH TEMPERATURE CAVITATION CREEP FAILURE

HEDL P-14-29
650°C BREACH
5×10^{22} n/cm^2
STRAIN = 0.8%

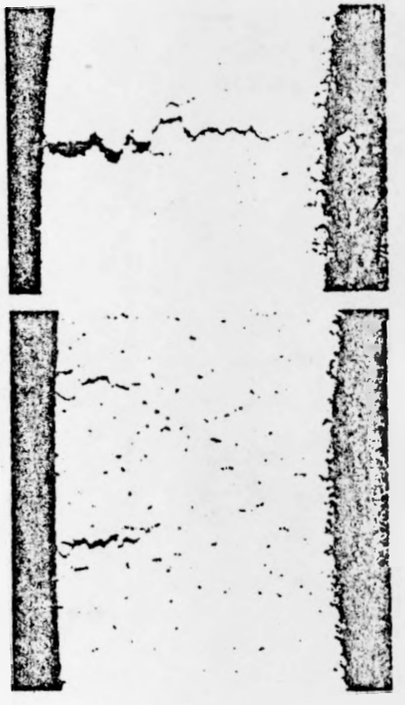

FIGURE 32, HIGH TEMPERATURE CAVITATION CREEP FAILURE

LOW TEMPERATURE INTERGRANULAR CRACK FAILURE

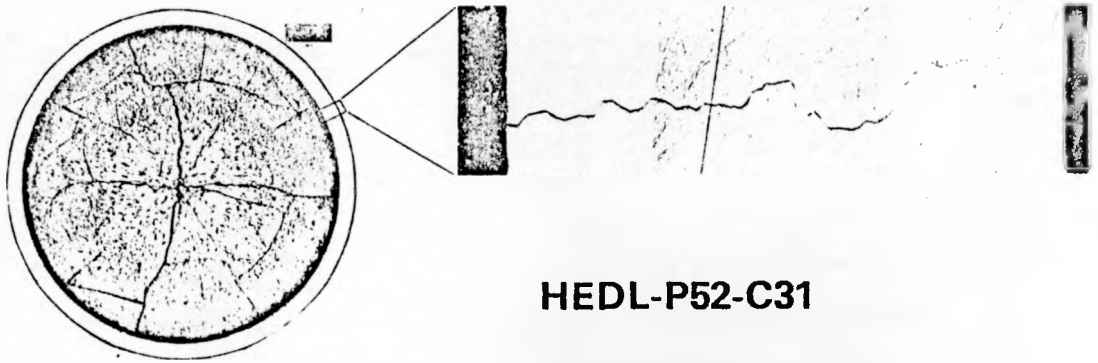

HEDL-P52-C31

427°C BREACH
7×10^{22} n/cm^2
STRAIN $\simeq$ 0.3%

FIGURE 33, LOW TEMPERATURE INTERGRANULAR CRACK FAILURE

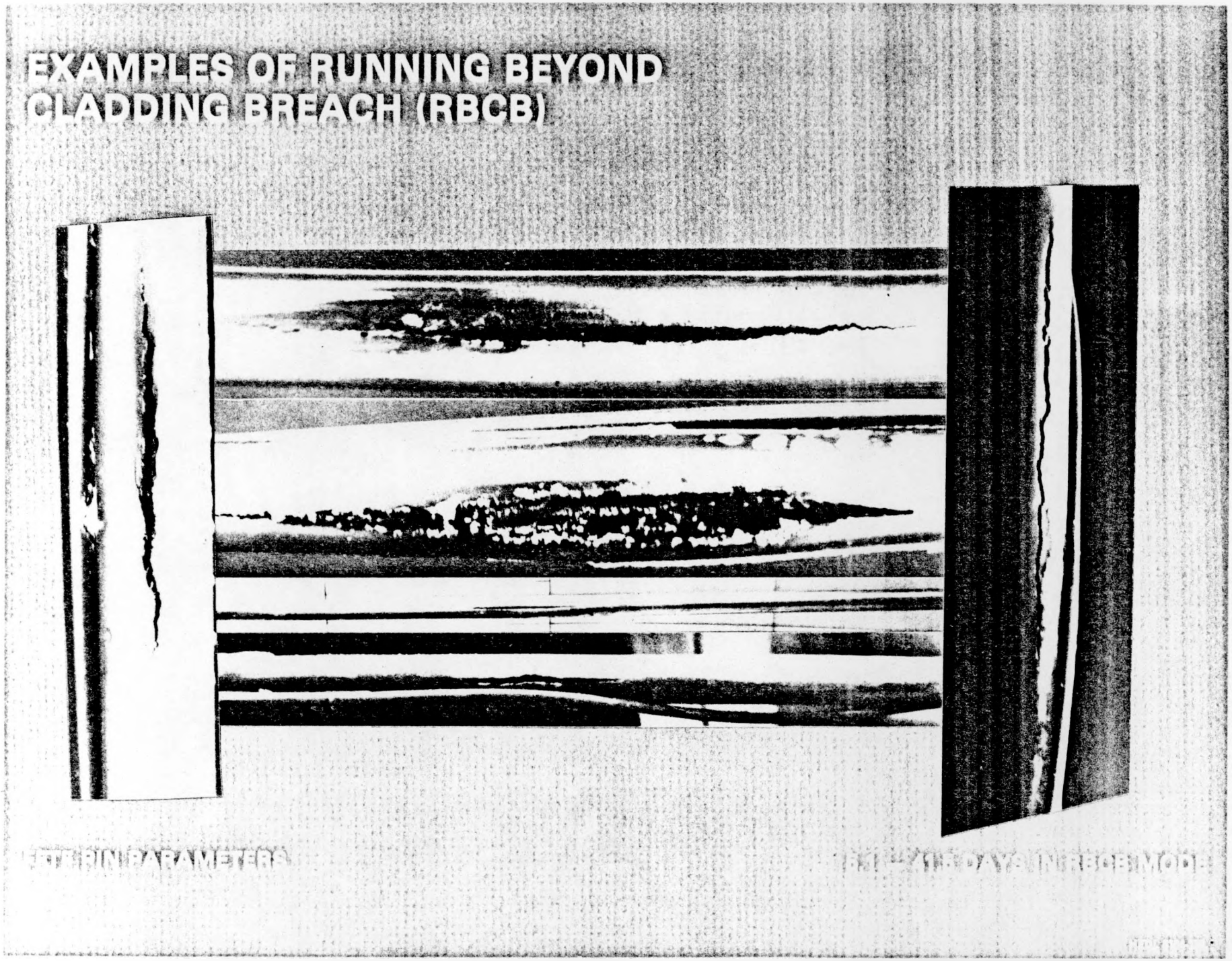

FIGURE 34, EXAMPLES OF RUNNING BEYOND CLADDING BREACH (RBCB)

cladding integrity limits testing

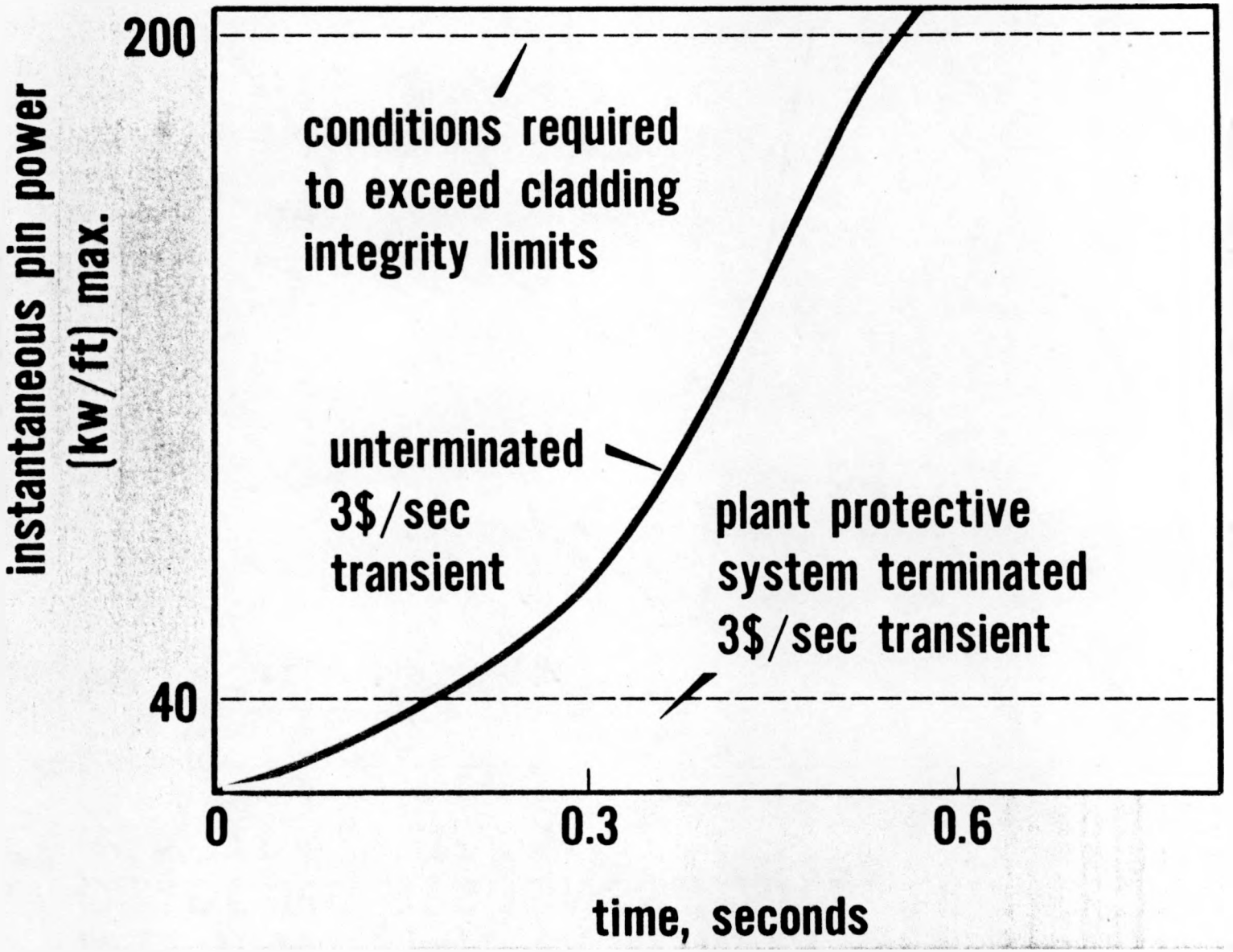

FIGURE 35, CLADDING INTEGRITY LIMITS TESTING

FFTF ROW 4 PIN AXIAL MIDPLANE CLADDING RESPONSE TO A 5¢/sec REACTIVITY RAMP

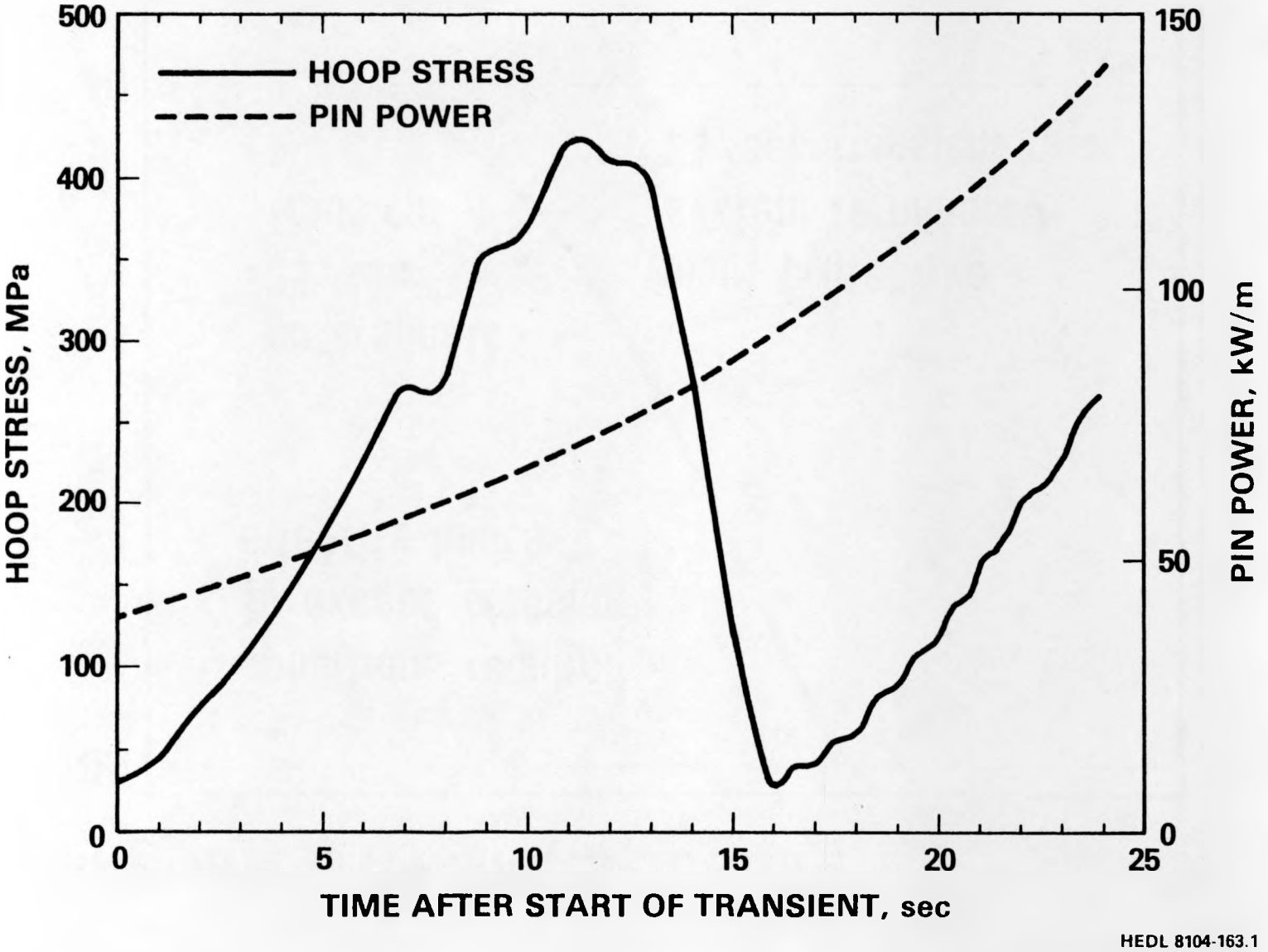

FIGURE 36, FFTF ROW 4 PIN AXIAL MIDPLANE CLADDING RESPONSE TO A 5¢/sec REACTIVITY RAMP

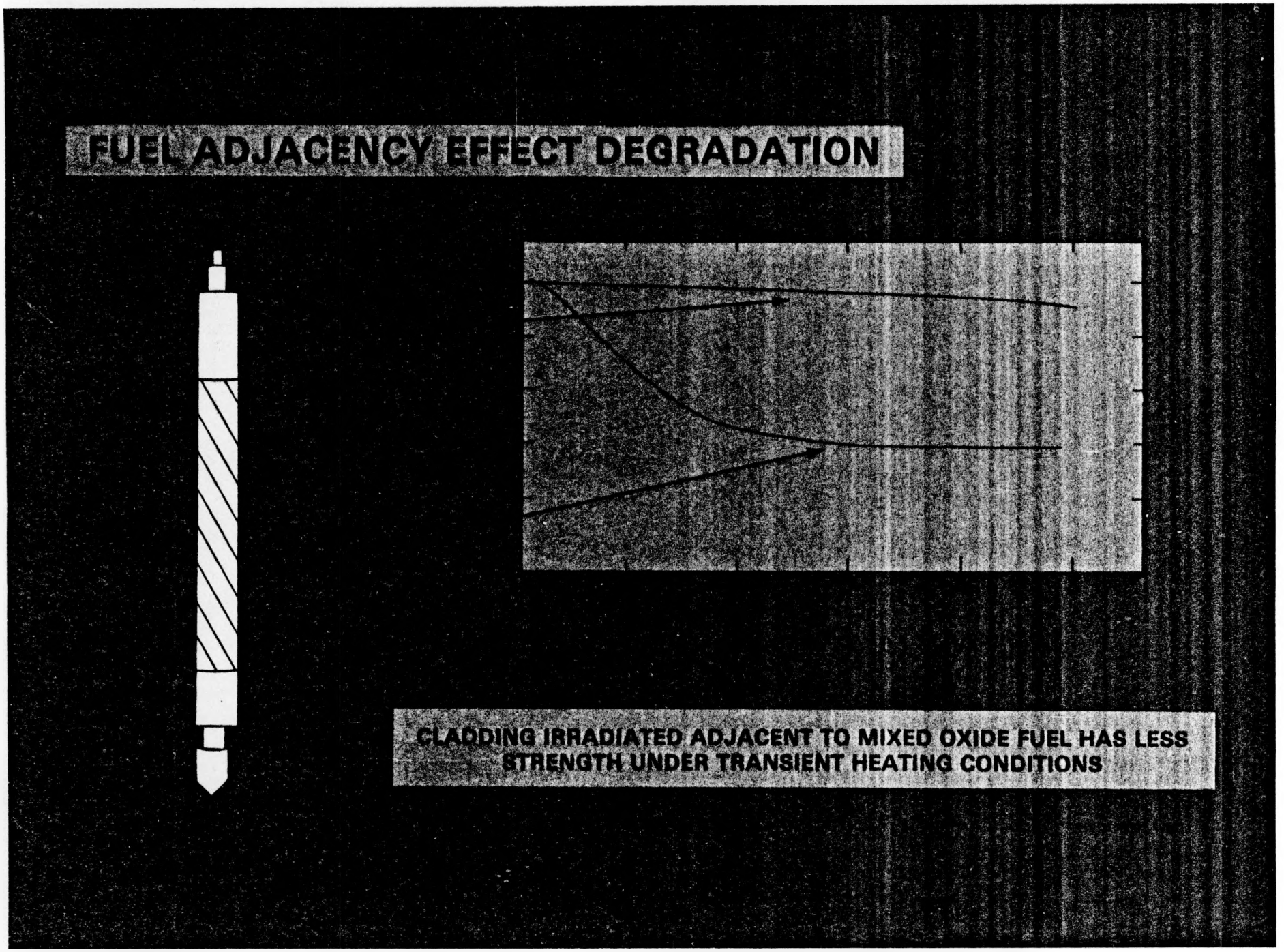

FIGURE 37, FUEL ADJACENCY EFFECT DEGRADATION